Chapter 1   Introduction

1-0 Preface

The determination of optical nonlinearities and their response times in semiconductor is great important to the practical applications of optical limiting devices and all-optical switching elements.   In the language of quantum mechanics, a virtual carrier lifetime can be defined from the uncertainty principle as $1/|\omega\text{-}\omega_g|$. Here, ω is the optical frequency, $\omega_g = E_g/\hbar$ with E_g being the band-gap energy of the solid and $\hbar$ the Planck's constant.   This equality means that in the transparency region where $\omega << \omega_g$, the response time is very fast ($<< 10^{-14}$ s) and can be regarded as essentially instantaneous.

The optical nonlinear response in the transparent region of semiconductors can be classified into two categories, namely, (1) third-order nonlinearities arising from bound-electronic effects and two photon absorption (TPA) and (2) free carrier nonlinearities due to the photoexcitation of free carriers.   Nonlinear refraction associated with the bound-electronic Kerr effect is described by $\Delta n = n_2 I$, where I is the light irradiance (W/cm^2) and n_2 (cm^2/W) is the optical Kerr coefficient of the solid. Many methods can be used to determine the nonlinear responses that will be described later.

1-1 Applications of $\chi^{(3)}$

A wide-band-gap semiconductor, such as GaN, ZnSe and ZnO, has been great deal of interest due to their nonlinear properties [1]. Among them, the exciton binding energy (~60 *meV*) of ZnO is much higher than that of ZnSe (20 *meV*) and GaN (27 *meV*). ZnO has the room-temperature band-gap of ~3.37*eV* (368 *nm*) and high excitonic gain and therefore can be used as UV or blue emitting materials [2-3]. Other important applications is also introduced as follows.

1-1-1 Ultrafast all-optical switching

In recent years, considerable research has gone into the study of all-optical switching devices in waveguides [4]. A material with a large n_2 (nonlinear refractive index) may be required by taking advantage of relatively high power densities and long interaction lengths. The intensity out of waveguide can be represented as

$$I_{trans} = I_{inc} \frac{C_1 C_2 e^{-\alpha L}}{1 + (\beta L_{eff} C_1 P_{inc} / A_{eff})}$$ where $L_{eff} \equiv (1 - e^{-\alpha L} / L)$, P_{inc} is the total peak laser

power incident upon the waveguide, I_{inc} is the incident laser intensity, I_{trans} is the transmitted intensity, and A_{eff} is an effective core area, which takes into account the mode profiles. In order to obtain all-optical switching within waveguide, a limitation $\dfrac{2\beta\lambda}{n_2} < 1$ (where β is the two photon absorption coefficient) is needed in terms of a geometry-independent criterion for avoiding large TPA-induced loss of the beam [5].

A pump and probe technique can be utilized to demonstrate an all-optical

switching which is based on nonlinear absorption.   The probe beam of wavelength 815 *nm* is absorbed by the intermediate state of the material when the pulsed pump beam is *off*.   In this experiment, the transmission intensity of the probe beam is low because of high linear absorption.   Exposure of the sample to the pump beam (665 *nm*), causes the depopulation of the ground state and increased population of the intermediate state. This induces a bleaching of the ground state to the intermediate state, causing the transmission intensity of the probe beam to increase, i.e., it is in the *on* state [6].

In a word, nonlinear properties of materials play an important role for optical devices in future.

1-1-2 Optical limiting

Nonlinear optical materials with large intensity-induced refractive index and absorption changes have strong potential application in the designs of the optical limiter, which can protect optical sensors and human eyes from laser damages.   In the optical limiting, the absorption of material increases following the increasing of exciting intensity.   This behavior is attributed to a reverse saturation mechanism which results from population of an excited state that has greater absorption cross section than that of the ground state.   The increase of the absorption coefficient of a nonlinear optical medium with increasing amount of incident light intensity can be used to limit the amount of energy transmitted by the medium.   The optical limiting in inorganic clusters is caused by strong nonlinear refraction, whereas the optical limiting in semiconductor structures is governed by two-photon absorption.

1-2 Review of $\chi^{(3)}$ measurement

In this section, several common experimental techniques, including four-wave mixing, Z-scan and pump-probe Z-scan for measuring nonlinear refraction and nonlinear absorption are described. Their merits and drawbacks will also be compared.

1-2-1 Degenerate Four wave-mixing (DFWM)

The first experimental demonstration of phase conjugation by DFWM was performed by Bloom and Bjorklund (1977). In this process, a lossless nonlinear medium characterized by a third-order nonlinear susceptibility $\chi^{(3)}$ is illuminated by two strong counterpropagating pump waves E_1 and E_2 and by a signal wave E_3. The pump waves are usually assumed to be plane waves, although in principle any wavefront structures and amplitudes complex conjugates of one another are used. In addition, an arbitrary wavefront of the signal wave is allowed. It can interpret physically that the DFWM in the phase conjugate geometry is automatically phase-matched. Fig. 1-1 shows one simple geometry for DFWM where two input beams (the forward and backward pumps) are counterpropagation. The process entails the annihilation of two pump photons and the creation of a signal and conjugate photon. The total input energy is $2\hbar\omega$ and the total input momentum is $\hbar(k_1 + k_2) = 0$, whereas the total output energy is $2\hbar\omega$ and the total output momentum is $\hbar(k_3 + k_4) = 0$. If the two pump beams are not exactly counterpropagation, then $\hbar(k_1 + k_2)$ does not vanish and the phase-matched

condition is not automatically satisfied [7].

One of the drawbacks of DFWM data analysis for third-order nonlinearities is that the intensity of phase conjugate wave is proportional to $\left|\chi^{(3)}\right|^2 = \left|\text{Re}\{\chi^{(3)}\}\right|^2 + \left|\text{Im}\{\chi^{(3)}\}\right|^2$ which is attributed to 2PA and n_2 both contributions. Separating the effects is difficult without performing additional experiments. Higher-order nonlinearities also can contribute, making separation of absorptive and refractive effects difficult.
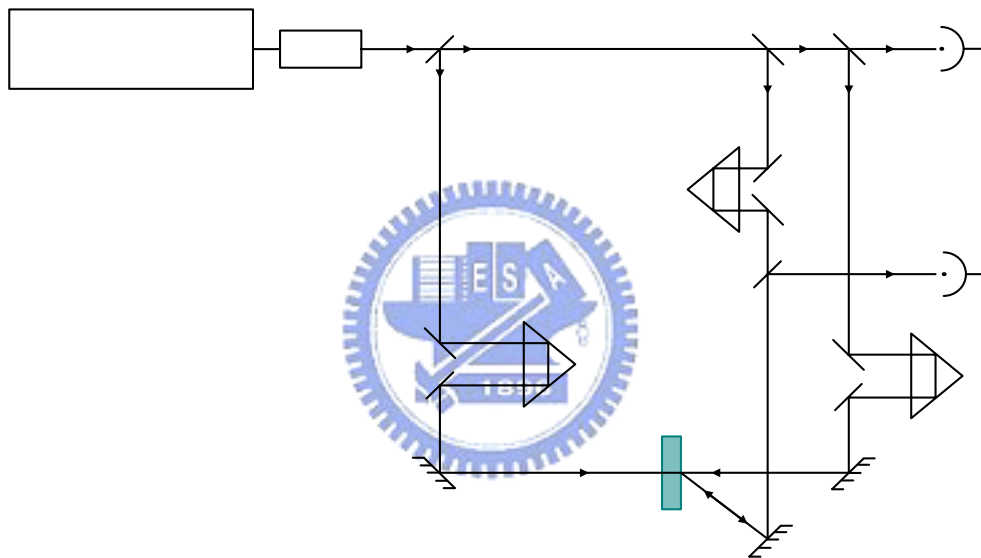

Fig. 1-1 DFWM geometry to allow temporal dynamics measurements. Detector D_2 monitors the conjugate beam energy.

1-2-2 Z-scan

Z-scan measurement was developed by Sheik-Bahae et al. in 1989 [8]. The method has gained rapid acceptance for separately measuring the nonlinear refraction and absorption due to the simplicity of setup and interpretation. Fig. 1-2 shows a standard Z-scan apparatus. The position Z dependent far field transmittance of the

sample through the aperture is monitored in a photodiode. For "thin" samples (i.e., $L \leq n_0 Z_0$ where n_0 is the linear index), all the information is theoretically contained with a scan range of $\pm Z_0$. Here Z_0 is the diffraction length of the focused beam defined as $\pi \omega_0^2 / \lambda$ for a Gaussian beam, where ω_0 is the focal spot size (half-width at the $1/e^2$ maximum in the irradiance).
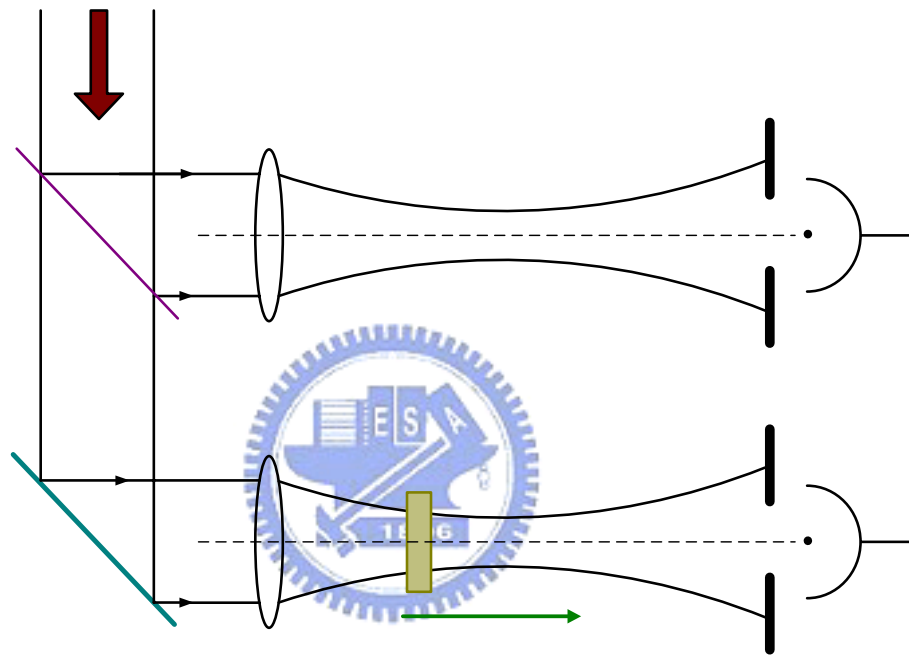

Fig. 1-2 Z-scan geometry with reference detector to minimize background and maximize the signal-to-noise ratio.

Fig. 1-3 shows a typical Z-scan measurement for S=1 that collects all the transmitted light and is insensitive to nonlinear refraction that shows a symmetric shape. Such a scheme, referred to as an "open aperture" Z-scan, is suited for measuring nonlinear absorption in the sample. The normalized transmittance shows a sharply declining in the focal point due to the maximal nonlinear absorption.
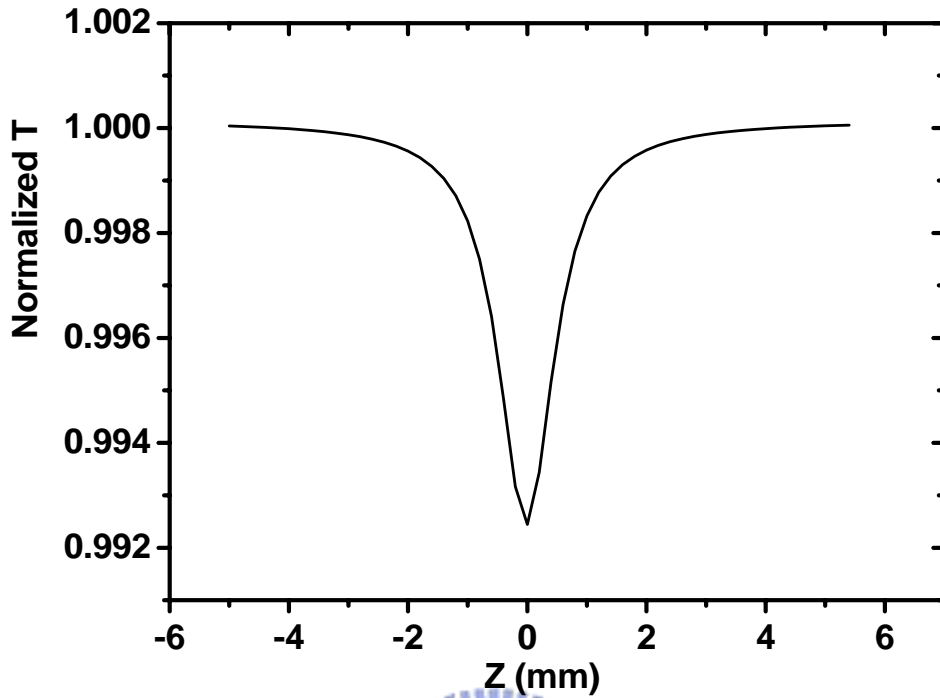
Fig. 1-3 A typical open aperture Z-scan signal for third order nonlinear absorption

Fig. 1-4 shows a typical closed aperture Z-scan due to the pure nonlinear refraction in which a self-focusing nonlinearity ($\Delta n > 0$) results in a valley-peak feature in the normalized transmittance (solid line) as the sample is moved away from the lens. Before the focal position of the lens, the self-focusing results in a greater far field divergence and a reduced aperture transmittance. While the sample placed after focus, the larger transmittance through the aperture is due to the reducing of the far field divergence. The opposite characterization is displayed by the dash line occurring for a self-defocusing nonlinearity, $\Delta n < 0$.

In order to obtain pure nonlinear refraction, a further division of the closed aperture Z-scan by the open aperture Z-scan data is performed. In this way, the absorptive and refractive nonlinearities can be separated without computer fitting of the Z-scans.
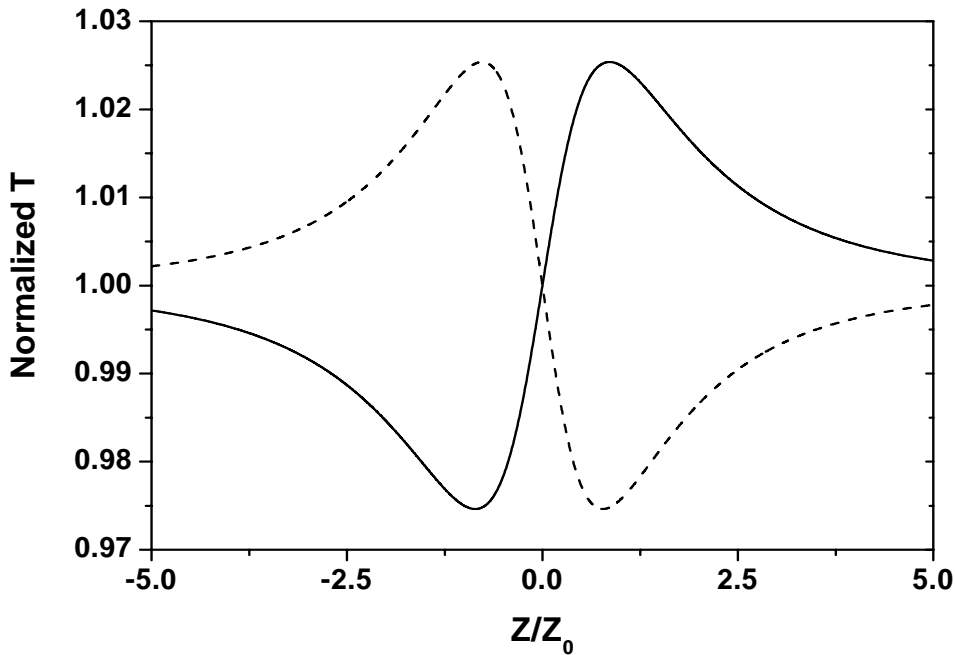
Fig. 1-4 Predicted Z-scan signal for positive (solid line) and negative (dashed line) nonlinear phase shifts.

1-2-3 Pump-probe Z-scan

Pump-probe techniques in nonlinear optics have been commonly employed to obtain the information that is not accessible in the single beam geometry. The most significant application of such techniques concerns the ultrafast dynamics of the nonlinear optical phenomena. There have been a number of investigations of Z-scan in a pump-probe scheme [9] [10] [11] whose general geometry is shown in Fig. 1-5 using the collinearly excitation and probe beams with the different polarization. After propagation through the sample, the probe beam through the far field aperture is separated by the polarization beam splitter and analyzed. The time-resolved studies can be performed in two fashions. In one scheme, the traditional Z-scans are performed at various fixed delays between pump and probe pulses. In the second

scheme, the sample is fixed at the peak or the valley position.   The transmittance of the probe beam is recorded at the various delay between the pump and probe beam. The analysis of the two-beam Z-scan is naturally more involved than that of a single beam Z-scan.   The measure signal depends not only on the parameters considered in the single-beam geometry but also on the parameters such as the pump-probe beam waist ratio and the possible focal separation due to chromatic aberration of the lens.
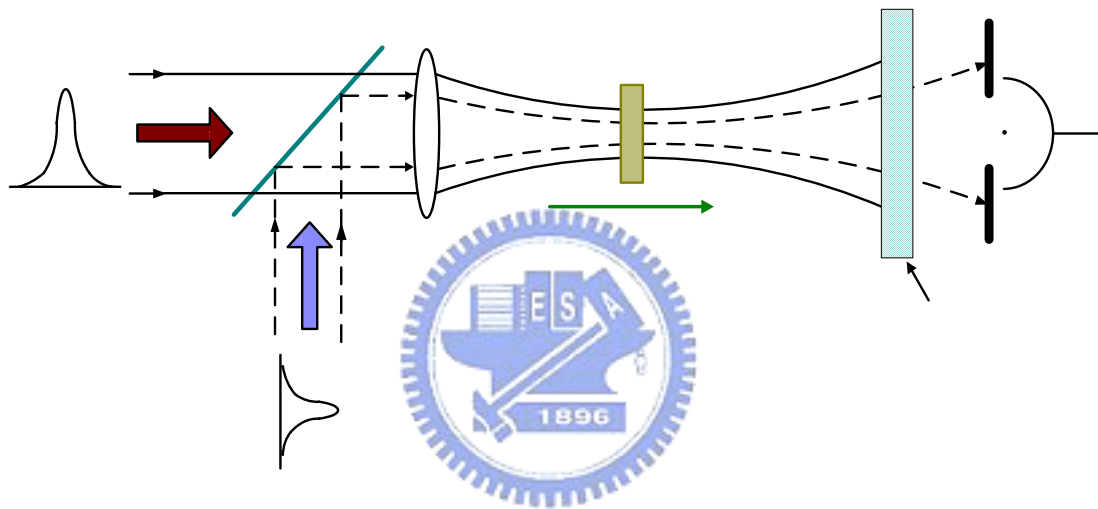

Fig. 1-5 Optical geometry for a two-color Z-scan.

1-3 Properties of ZnO

1-3-1 merits of ZnO

Zinc oxide (ZnO) is a II-VI semiconductor with a wide bandgap of 3.37eV, melting point of around 2250 ^0K.   It is a self-activated crystal of hexagonal wurtzite structure with lattice constant of a=0.3249 nm and c=0.5207 nm in the space group C_{6v}^4.   The deposited thin film usually belongs to c-axis-oriented textures.   The notable properties of ZnO are due to its large nonlinearity at room temperature and a high exciton binding energy (~60 meV) that is much higher than that of ZnSe (20 meV) and GaN (27 meV).   Furthermore, the high exciton binding energy permits excitonic recombination even at room temperature.   Due to these properties, ZnO can be used as UV or blue emitting materials.   In addition to optical transparency throughout the visible region and the large piezo-optic and piezoelectric effects in films with c-axis oriented, trivalent cation-doped ZnO exhibits marked electrical conductivity. Therefore, ZnO thin film can be a better choice for photo-electronic device applications [12].   Besiedes, ZnO are attractive as a candidate for ultraviolet optoelectronic device applications [13].

1-3-2 Second and Third harmonic generation (SHG and THG) of ZnO thin film

There has been much interested in the development of new nonlinear optical materials for potential application in integrated optics.   Impressive progress has been

made in nonlinear optical waveguides. However, these waveguides are fabricated by expensive single nonlinear-optical-crystals. It is desirable to fabricate thin films with large nonlinear optical response. Large second-order nonlinear optical response from ZnO thin films deposited on sapphire substrates by pulsed laser ablation has been observed. The second-order susceptibility $\chi_{zzz}^{(2)}$ of the 18*pm/V* is larger than the value for bulk single-crystal ZnO [14]. By comparing the second harmonic signal generated from films with different crystallinity and thickness, a significant second harmonic signal is generated at grain boundaries and interfaces [15] that is not well understood and requires further study. Because the second harmonic signal from the film is not dependent on the deposition method or substrate material, i.e. insensitivity to production details, so that it can be used for a variety of applications [14].

Nonlinear optical conversion efficient is studied in thin films of wide-bandgap materials. Very high conversion efficiency of the third-harmonic radiation is achieved by a pulsed-laser-deposition of the submicron-thick nanocrystalline ZnO film on a fused silica [16] with an unamplified femtosecond Cr^{4+}:forstesrite laser as the exciting source. Furthermore, nonresonant nonlinear optical susceptibilities of ZnO may be significantly affected by the small size of nanocrystals. For extremely thin films in which the film thickness is much less than the coherence length, $l_{coh} = 2\pi / \Delta k$, the intensity of the third harmonic signal is proportional to the square of the film thickness. Therefore, the high efficiency of nonlinear optical conversion makes it possible to use thin films of nanostructured ZnO for third-order autocorrelation measurements of weak pulses.

1-4 Aim of this thesis

In this thesis we concentrate on the resonant behaviors of half bandgap and exciton of ZnO thin film and further discuss the nonlinearity induced by thermal-optical effect. Previous measurements of ZnO material have showed a larger two photon absorption coefficient of $8.6cm/GW$ for polycrystalline ZnO than that ($4.2cm/GW$) of single crystal ZnO bulk with excitation wavelength of $532nm$ [17]. Besides, in GaN thin film the huge enhancement of two photon absorption induced by exciton effect has been investigated [18]. It has a more than one hundred times enhancement near exiton resonance. As a result of large exciton binding energy and electron-hole Coulomb interaction of ZnO which is similar to GaN, we believe the resonant behaviors of ZnO thin film are the same with GaN thin film. Therefore, we performed the Z-scan measurements with excitation wavelength of near infrared. To our knowledge, this is the first time for ZnO thin film measurements with excitation wavelength near half bandgap and compares with the results of near band edge. Besides, the nonlinearity induced by thermal-optical effect is important for using high repetition rate laser. The detail is all showed in chapter 4.

In chapter 2, we briefly describe the nonlinearity induced by bound electronic, free carrier and thermal-optical effects in Z-scan measurement and introduce a two-band model to derive the nonlinear absorption and refraction coefficients. All experimental setup is showed in chapter 3 and final conclusions and perspective are both given in chapter 5.

Chapter 2   Theoretical basis

2-1 Analysis of Z-scan

2-1-1 Bound-electronic and Free-carrier nonlinearity

Much work has been done in investigating the propagation of intense laser beams inside a nonlinear material and ensuing nonlinear refraction.   In considering only a cubic nonlinearity, the index of refraction n is expressed in terms of nonlinear indexes n_2 (esu) or γ (m^2/W) through

$$n = n_0 + \frac{n_2}{2}\left|E\right|^2 = n_0 + \gamma I \Rightarrow \Delta n(I) = \gamma I, \tag{1}$$

where n_0 is the linear index of refraction, E is the peak electric field (cgs), and I denotes the irradiance (MKS) of the laser beam within the sample.   Furthermore, n_2 and γ are related by the conversion formula $n_2\ (esu) = (\frac{cn_0}{40\pi})\gamma\ (m^2/W)$, where c (m/s) is the speed of light in vacuum.

Assuming a TEM$_{00}$ Gaussian beam of beam waist w_0 traveling in the $+z$ direction and the sample length is small enough that changes in the beam diameter within the sample due to either diffraction or nonlinear refraction can be neglected, the medium is regarded as "thin", in which case the self refraction process is referred to as "external self-action".   With above conditions and using the slowly varied envelope approximation (SVEA), a pair of simple equation is obtained:

$$\begin{cases} \dfrac{d\Delta\phi}{dz'} = \dfrac{2\pi}{\lambda}\Delta n(I) \\[2mm] \dfrac{dI}{dz'} = -\alpha(I)I \end{cases} \tag{2}$$

where I is the amplitude, ϕ is phase of the electric field, z' is the propagation depth in the sample and $\alpha(I)$, in general, includes linear and nonlinear absorption terms. In closed aperture case and only consider the linear absorption $\alpha(I) = \alpha$, (2) is solved to give the phase shift $\Delta\phi$ at the exit surface of the sample which simply follows the radial variation of the incident irradiance at a given position of the sample z. Thus,

$$\Delta\phi(z,r,t) = \Delta\phi_0(z,t)\exp(-\frac{2r^2}{w^2(z)})$$ (3)

with

$$\Delta\phi_0(z,t) = \frac{\Delta\Phi_0(t)}{1 + z^2/z_0^2}$$ (4)

$\Delta\Phi_0(t)$, the on-axis phase shift at the focus, is defined as

$$\Delta\Phi_0(t) = k\Delta n_0(t)L_{eff}$$ (5)

where $L_{eff} = (1-e^{-\alpha L})/\alpha$, with L the sample length and α the linear absorption coefficient. The complex electric field exiting the sample E_e now contains the nonlinear phase distortion

$$E_e(r,z,t) = E(r,z,t)e^{-\alpha L/2}e^{i\Delta\phi(r,z,t)}$$ (6)

where $E(r,z,t)$ is the electric field of incident into sample. By using Huygen's principle, one can obtain the far-field pattern of the beam at the aperture plane through a zeroth-order Hankel transformation of E_e. Here, a more convenient treatment applicable to Gaussian input beam which is referred to as the "Gaussian decomposition" (GD) method is used. In which the complex electric field at the exit plane of the sample is decomposed into a summation of Gaussian beams through a Taylor series expansion of the nonlinear phase term $e^{i\Delta\phi(r,z,t)}$ in (6). That is,

$$e^{i\Delta\phi(r,z,t)} = \sum_{m=0}^{\infty} \frac{[i\Delta\phi_0(z,t)]^m}{m!}e^{-2mr^2/w^2(z)}$$ (7)

Each Gaussian beam can be simply propagated to the aperture plane where they will be resumed to reconstruct the beam and resulted in a compound electric field

of $E_a(r,z,t)$. The transmitted power through the aperture is obtained by spatially integrating $E_a(r,z,t)$ up to the aperture radius r_a, giving

$$P_T(\Delta\Phi_0(t)) = c\varepsilon_0 n_0 \pi \int_0^{r_a} |E_a(r,z,t)|^2 \, r dr \qquad (8)$$

where ε_0 is the permittivity of vacuum. Including the pulse temporal variation, the normalized Z-scan transmittance $T(z)$ can be calculated as

$$T(z) = \frac{\int_{-\infty}^{\infty} P_T(\Delta\Phi_0(t)) dt}{S \int_{-\infty}^{\infty} P_i(t) dt} \qquad (9)$$

where $P_i(t) = \pi\omega_0^2 I_0(t)/2$ is the instantaneous input power and $S = 1 - e^{-2r_a^2/\omega_a^2}$ is the aperture linear transmittance, with ω_a denoting the beam radius at the aperture in the linear regime. If the nonlinearity is cubic, small phase change and $d \gg z_0$ (far-field condition), the on-axis electric field at the aperture plane can be obtained by letting $r = 0$. Following such simplifications, the normalized Z-scan transmittance can be written as

$$T(z,\Delta\Phi_0) = \frac{|E_a(r=0,z,\Delta\phi_0)|^2}{|E_a(r=0,z,\Delta\phi_0=0)|^2} \simeq 1 + \frac{4x}{(x_2+9)(x_2+1)}\Delta\Phi_0 \qquad (10)$$

where $x = z/z_0$. (10) is the fitting formula for nonlinearity due to nonlinear refraction.

Next, considering the nonlinear absorption such as two photon absorption (TPA), (2) will be reexamined after the substitution:

$$\alpha(I) = \alpha + \beta I \qquad (11)$$

Following the same procedures, the total transmitted fluence in the case of open aperture can be showed as follows:

$$P(z,t) = P_i(t)e^{-\alpha L}\frac{\ln[1+q_0(z,t)]}{q_0(z,t)} \qquad (12)$$

where $q_0(z,t) = \beta I_0(t)L_{eff}/(1+z^2/z_0^2)$ and $P_i(t) = \pi w_0^2 I_0(t)/2$. For a temporally

Gaussian pulse, (12) can be time integrated to give the normalized energy transmittance

$$T(z, S = 1) = \frac{1}{\sqrt{\pi} q_0(z,0)} \cdot \int_{-\infty}^{\infty} \ln[1 + q_0(z,0)e^{-\tau^2}] d\tau \qquad (13)$$

For $|q_0| < 1$, this transmittance can be expressed in terms of the peak irradiance in a summation form more suitable for numerical evaluation:

$$T(z, S = 1) = \sum_{m=0}^{\infty} \frac{[-q_0(z,0)]^m}{(m+1)^{3/2}} \qquad (14)$$

(14) is the fitting formula for nonlinearity resulted from two photon absorption.

At higher irradiance level the nonlinear refraction caused by 2PA-generated free charge carriers, an effective fifth-order nonlinearity, becomes significant. Thus the change of refractive index will become:

$$\Delta n \simeq \gamma I_0 + C \sigma_r I_0^2 \qquad (15)$$

where $C = 0.23(\beta t_0 / \hbar \omega)$ for low linear absorption ($\alpha_0 L < 0.2$), t_0 is the pulse width. The analytic procedures which involved free carriers are the same as above descriptions.

2-1-2 Thermal-optical nonlinearity

The effects on Z-scan measurements of thermal-optical nonlinearities due to cumulative heating of the sample have been investigated [17] [19]. The thermal-optical nonlinearities occurs while the exciting pulse trains whose spacing is shorter than the thermal characteristic time $t_c = w^2 / 4D$, where D ($cm^2 s^{-1}$) is the thermal diffusion coefficient of the sample and w is the laser spot size. In general, t_c is greater than $40 \mu s$ in typical Z-scan measurement so that thermal-optical

nonlinearities condition met while the repetition rate of the pulses is greater than a few tens of KHz. The model of the thermal-optical nonlinearities in the Z-san measurement is presented which takes into account the absorption processes involving an arbitrary number of photons as the sources of nonlinearity [20]. Conversely, very weak nonlinear absorption coefficients can be measured exploiting the effect of cumulative heating when using high repetition rate lasers.

Two distinct parts must be considered in the modeling of thermo-optical effects: first, the temperature profile generated by the absorption of the light in the sample is calculated. Then, we estimate the effect of the thermo-optical phase shift on the laser beam propagation after the sample. The energy density absorbed per second in an absorption process involving q photons can be written as

$$U(z,r) = qh\upsilon N\sigma f \int I^q(z,r,t)dt,$$ (16)

where $h\upsilon$ is the photon energy (J), N is the density of absorbing center (cm^{-3}), σ is the multiphoton absorption cross section ($cm^{2q} s^{q-1}$), f is the repetition rate of laser, $I(z,r,t)$ is the distribution of photon flux ($cm^{-2} s^{-1}$) of a single laser pulse and the integral is over the pulse duration. Under approximation of an optically thin film sample, the photon distribution inside the sample is:

$$I(z,r,t) = \left[\frac{2P(t)}{\pi\omega^2(z)}\right]\exp(\frac{-2r^2}{\omega^2(z)}),$$ (17)

where $P(t)$ (s^{-1}) is proportional to the power of the pulse, and $\omega(z)$ is the laser beam spot size at the sample location z. Incorporating (16) and (17), the heat generated per unit length between r and $r+dr$ in the unit time is

$$U(z,r)2\pi rdr = qh\upsilon N\sigma f(\frac{2}{\pi\omega^2(z)})^q \exp\left[\frac{-2qr^2}{\omega^2(z)}\right]H(q)2\pi rdr,$$ (18)

where

$$H(q) = \int P^q(t)dt$$ (19)

is the integration over the pulse duration. Therefore, the temperature profile can be derived as

$$\Delta T(z,r,t) = qh\upsilon N\sigma f\left[\frac{2}{\pi\omega^2(z)}\right]^{q-1}\frac{H(q)}{4\pi\kappa q}\times\left\{Ei\left[\frac{-2qr^2}{\omega^2(z)}\right]-Ei\left[\frac{-2qr^2}{\omega^2(z)}\frac{1}{1+2qt/t_c}\right]\right\},(20)$$

where κ $(W\ cm^{-1}\ K^{-1})$ is the thermal conductivity of the sample, $Ei(x)$ is the exponential-integral function as defined for example by Gradshteyn and Ryzhik [21]. The temperature profile (20) will produce a refraction index profile through the thermo-optical coefficient dn/dT (K^{-1}) of the sample. If G_i is the Gaussian beam amplitude at the entrance of plane of the sample, the beam amplitude at the exit plane G_0 is given by:

$$G_0(z,r,t) = G_i(z,r)\exp\left[-ik\frac{dn}{dT}\Delta T(z,r,t)L\right],\tag{21}$$

where k (cm^{-1}) is the wavevector of the light and L (cm) the sample length. The thermal lens signal can be obtained from on-axis $(r=0)$ intensity through the propagation of the field (21) from the rear face of the sample to the detector plane $z=d$ and normalized to the intensity for $t=0$ (when there is no thermal lensing). The curve obtained by plotting the thermal lens signal at fixed time as a function of the position of the sample due to a thermo-optical nonlinearity. Therefore, the time-dependent Z-scan trace from the thermo-optical nonlinearity can be obtained for different measuring time. The signal can be calculated by a numerical evaluation of the propagation integral as

$$E(0,z,t) = \frac{2\pi}{i\lambda(d-z)}J_0(0)\int_0^\infty r'G_0(z,r',t)\times\exp\left[\frac{i\pi r'^2}{\lambda(d-z)}\right]dr',\tag{22}$$

where J_0 is a Bessel function, λ the wavelength of light, and G_0 the field at the output face of the sample, given by equation (21).

In order to obtain an analytical form, the Fraunhofer region approximation is

used here for propagation integral (detector in the far field) and the thermo-optical phase factor is linearized by a first-order series expansion of the exponential in equation (21). When the temperature profile (20) is used, the parameter ϑ that represents the thermal lens strength defined by Sheldon $et\ al$ is generated to account for multiphoton processes of arbitrary order q [22]:

$$\vartheta(q) = kL \frac{qh\upsilon H(q)N\sigma f}{2\pi\kappa} \frac{dn}{dT} \left(\frac{2}{\pi\omega_0^2} \right)^{q-1}, \tag{23}$$

where ω_0 is the spot size of the laser at the focus. Then, the on-axis electric field on the detector when the sample is in the normalized coordinate position $\xi = z/z_0$ is

$$E(0, \xi, t) = const \times \left[1 - i \frac{\vartheta(q)}{2q(1+\xi^2)^{q-1}} \ln \frac{(1+i\xi)(1+2qt/t_c)+2q}{1+2q+i\xi} \right]. \tag{24}$$

Therefore, the normalized signal intensity calculated by neglecting terms of order ϑ^2 is

$$\frac{I(\xi,t)}{I(\xi,0)} = 1 + \frac{\vartheta(q)}{q} \frac{1}{(1+\xi^2)^{q-1}} \times \tan^{-1} \left(\frac{2q\xi}{\left[(2q+1)^2 + \xi^2 \right] \frac{t_c(\xi)}{2qt} + 2q + 1 + \xi^2} \right) \tag{25}$$

that have explicitly stated the dependence of t_c on the sample position. Eq. (25) is the expression for the time-dependent Z-scan curves generated by thermo-optical effects. Note that if several absorption processes of different order, possibly due to different absorbing centers, are active, the resulting signal will be the sum of the ones due to each process because of the linearity of this model.

2-2 Dispersion of bound-electronic nonlinearities: Two-Band Model

A two-band model is used to calculate the scaling and spectrum of the nondegenerate nonlinear absorption $\Delta\alpha(\omega_1;\omega_2)$. From this, the bound-electronic nonlinear refraction index n_2 is obtained using a Kramers-Krönig (KK) transformation. It has experimentally showed an excellent agreement with theoretical calculation for $\Delta\alpha(\omega_1;\omega_2)$ and n_2 in semiconductors and wide-gap optical solids [23] [24]. Here, a model that includes the ac Stark effect and the electronic Raman effect as well as 2PA is presented.

2-2-1 Nonlinear absorptions

The second order perturbation theory is used here to deal with two photon absorption processes. Beginning, the dipole approximation for the radiation interaction Hamiltonian is taken and then the transition rate will be calculated using an S-matrix formalism [25]

$$S = \frac{i\pi}{\hbar}\frac{e\hat{a}\cdot p_{vc}}{m_0 c}\sum_{m,n=-\infty}^{\infty}J_m(\eta_1)J_n(\eta_2)\cdot\{A_{01}[\delta((m+1)\omega_1+n\omega_2+\omega_{vc})+\delta((m-1)\omega_1+n\omega_2+\omega_{vc})]+A_{02}[\delta(m\omega_1+(n+1)\omega_2+\omega_{vc})+\delta(m\omega_1+(n-1)\omega_2+\omega_{vc})]\}$$ (26)

From the S-matrix description, transition rate can be determined to define the absorption coefficient. The resulting expression for a change of absorption in nondegenerate case using the second-order perturbation approach is

$$\Delta\alpha(\omega_1,\omega_2) = 2K\frac{\sqrt{E_p}}{n_{01}n_{02}E_g^3}F_2(x_1,x_2)I_2 = \beta I_2 .$$ (27)

The function F_2 is a function of the ratio of the photon energy $\hbar\omega$ to E_g (i.e. denoting the optically coupled states). The different form of the functional F_2 depends on the assigning band structure and the intermediate states. E_p is nearly material independent and possesses a value $E_p \approx 21eV$ for most direct band gap semiconductors, and K is a material-independent constant that is defined as

$$K = \frac{2^9 \pi}{5} \frac{1}{(4\pi\varepsilon_0)^2} \frac{e^4}{\sqrt{m_0 c^2}} . \tag{28}$$

The value of K is 1940 whose units depend on β in *cm/GW*, and E_g and E_p in *eV*.

The absorption spectral function $F_2(x_1, x_2)$ can result from two photon absorption, Raman and ac Stark effect that is presented in table I. In Raman transition, an electron is excited from the valence band into the conduction band via absorption of a photon at $\hbar\omega_1$ and emission a photon at $\hbar\omega_2$ ($\omega_1 > \omega_2$, stoke) and vice versa ($\omega_1 > \omega_2$, anti-stoke). The two photon absorption occurs when the sum of the frequencies is equal to the bandgap. However, the Raman term turns on when the difference of the frequencies is equal to the bandgap so that one frequency must exceed the bandgap. Absorption coefficient can also be changed due to a shift in bandgap as a result of the ac Stark effect. For example, a change in the linear absorption of the light with the frequency ω_1 occurs when the bands are shift due to the ac Stark effect caused by the exciting light with frequency ω_2 near band-edge. Two different kinds of ac Stark effect can be occurred. If the transition of the $\omega1$ is the conduction (or valence) band to itself, is termed the linear Stark effect. Otherwise, the transition from the conduction band to the valence band, it is termed the quadratic Stark effect. The same condition can be generated in the ac Stark effect depending on $\hbar\omega_1 > E_g$ or

$\hbar\omega_2 > E_g$.

Contribution	$F_2(x_1,x_2)$
2-photon absorption $(x_1 + x_2 > 1)$	$\dfrac{(x_1 + x_2 - 1)^{3/2}}{2^7 x_1 x_2^2}(\dfrac{1}{x_1} + \dfrac{1}{x_2})^2$
Raman ($x_1 - x_2 > 1$)	$\dfrac{(x_1 - x_2 - 1)^{3/2}}{2^7 x_1 x_2^2}(\dfrac{1}{x_1} - \dfrac{1}{x_2})^2$
AC Stark ($x_1 > 1$)	$-\dfrac{1}{2^9 x_1 x_2^2 (x_1 - 1)^{1/2}}\left[\dfrac{x_1}{x_1^2 - x_2^2} - \dfrac{2(x_1 - 1)(x_1^2 + x_2^2)}{(x_1^2 - x_2^2)^2} + \dfrac{8(x_1 - 1)^2}{x_2^2}\right]$

Table I Contributions to the nonlinear absorption spectral function $F_2(x_1, x_2)$

2-2-2 Nonlinear refraction

In general, the nondegenerate refraction index change $\Delta n(\omega_1; \omega_2)$ can be evaluate by the Kramers-Krönig dispersion relation

$$\Delta n(\omega_1; \omega_2) = \frac{c}{\pi}\int_0^\infty \frac{\Delta\alpha(\omega'; \omega_2)}{\omega'^2 - \omega_1^2}d\omega' . \tag{29}$$

From Eq. (29), the nonlinear refraction can be derived as follows

$$n_2(\omega_1, \omega_2) = K'\frac{\sqrt{E_p}}{n_{01}n_{02}Eg^4}G_2(x_1, x_2), \tag{30}$$

where $K' = \dfrac{\hbar c K}{2} = \dfrac{2^4}{5\pi}\dfrac{\hbar e^4}{\varepsilon_0^2\sqrt{m_0 c}} = 1.5\times 10^{-8}$, and E_g and E_p are defined in eV. The dispersion function G_2 is given by

$$G_2(x_1; x_2) = \frac{2}{\pi}\int_0^\infty \frac{F_2(x'; x_2)}{x'^2 - x_1^2}dx' . \tag{31}$$

In Eq. (30), the linear refractive index n_0 has neglected the dispersion effect. Therefore, in order to determine of the n_2, the Eq. (31) is the only function needed to be evaluated for the various contributions of the nondegenerate absorption $F_2(x_1, x_2)$.

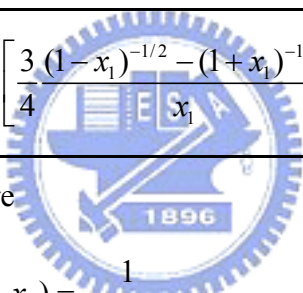Table II present the different contributions to dispersion function G_2.

Contribution	$G_2(x_1,x_2)$
2PA	$H(x_1,x_2)+ H(-x_1,x_2)$
Raman ($x_1 - x_2 > 1$)	$H(x_1,-x_2)+ H(-x_1,-x_2)$
AC Stark ($x_1 > 1$)	
$x_1 \neq x_2$	$\dfrac{1}{2^9 x_1^2 x_2^2}\left[\begin{array}{l} -\dfrac{1}{2}-\dfrac{4}{x_1^2}+\dfrac{4}{x_2^2}-\dfrac{x_2^2}{x_1}\dfrac{[(1-x_2)^{-1/2}-(1+x_1)^{-1/2}]}{x_1^2-x_2^2} \\[2mm] +\dfrac{2x_1^2(3x_2^2-x_1^2)}{x_2^2(x_1^2-x_2^2)^2}[(1-x_2)^{-1/2}-(1+x_2)^{-1/2}] \\[2mm] -\dfrac{2x_2^2(3x_1^2-x_2^2)}{x_1^2(x_1^2-x_2^2)^2}[(1-x_1)^{-1/2}-(1+x_1)^{-1/2}] \end{array}\right]$
$x_1 = x_2$	$\dfrac{1}{2^9 x_1^4}\left[\dfrac{3}{4}\dfrac{(1-x_1)^{-1/2}-(1+x_1)^{-1/2}}{x_1}-\dfrac{(1-x_1)^{-3/2}+(1+x_1)^{-3/2}}{8}-\dfrac{1}{2}\right]$
	Where $H(x_1,x_2)=\dfrac{1}{2^6 x_1^4 x_2^4}$ $\times\left[\begin{array}{l} \dfrac{5}{16}x_2^3 x_1^2+\dfrac{9}{8}x_2^2 x_1^2-\dfrac{9}{4}x_2 x_1^2-\dfrac{3}{4}x_2^3-\dfrac{1}{32}x_2^3 x_1^2(1-x_1)^{-3/2} \\[2mm] +\dfrac{1}{2}(x_2+x_1)^2[(1-x_2-x_1)^{3/2}-(1-x_1)^{3/2}] \\[2mm] -\dfrac{3}{16}x_2^2 x_1^2[(1-x_1)^{-1/2}-(1-x_2)^{-1/2}]+\dfrac{3}{2}x_2 x_1^2(1-x_2)^{1/2} \\[2mm] +\dfrac{3}{2}x_2^2 x_1(1-x_1)^{1/2}+\dfrac{3}{4}x_2(x_2^2+x_1^2)(1-x_1)^{1/2} \\[2mm] -\dfrac{3}{8}x_2^3 x_1(1-x_1)^{-1/2}+\dfrac{1}{2}(x_2^2+x_1^2)[(1-(1-x_2)^{3/2}] \end{array}\right]$

Table II Contributions to the nondegenerate dispersion function $G_2(x_1, x_2)$.

The individual contributions to the dispersion function G_2 as a function of frequency are shown in Fig. 2-1. It can be seen that the most significant contribution

to the spectral dependent of G_2 arises from the two photon absorption term and the quadratic Stark term becomes dominant only close to the band edge. The linear Stark term arising from the self-coupling of the bands is insignificant compared to the quadratic term.

Moreover, if electron-hole Coulomb interaction is included by multiplying the F_2 function with a generalized exciton enhancement factor as described by Sheik-Bahae et al. [24]. It will further improve the agreement between theory and experiment.
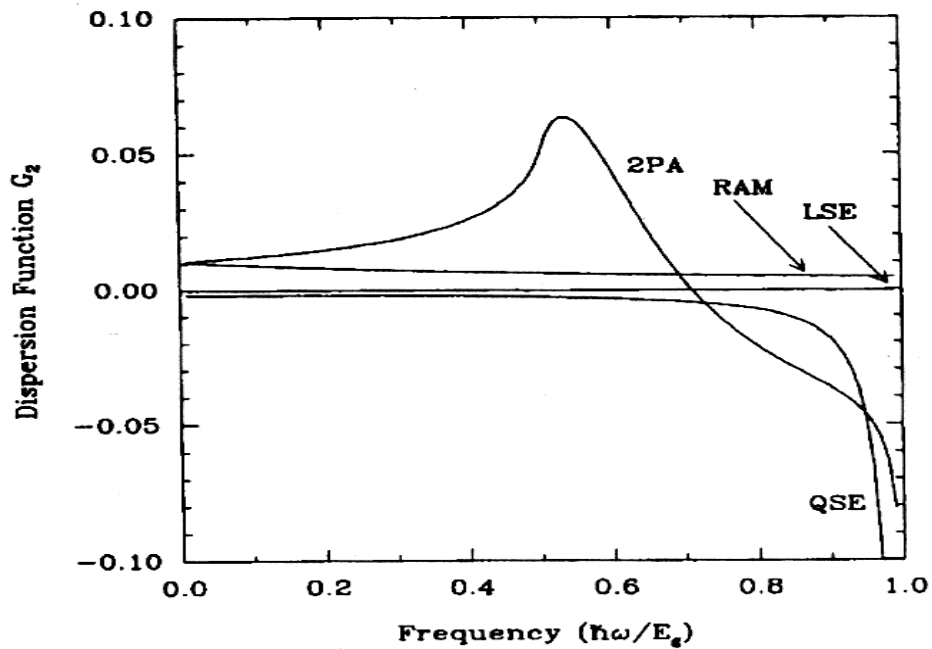
Fig. 2-1 Frequency dependence of the various contributions to the dispersion function.

Chapter 3　Experiments

3-1 Photoluminescence and transmission spectra

A UV He-Cd laser (Kimmon IK5552R-F) operating at wavelength 325nm is utilized as the pumping source for Photoluminescence (PL).　Fig. 3-1 shows the block diagram of PL detection system, it includes the reflective mirror, focusing and collecting lenses, and the single-grating monochromators (TRIAX 320) with a photo-multiplier tube (PMT-HVPS) which is equipped with a photon counter.　The TRAIX 320 monochromator has three selectable gratings of 600, 1200 and 1800 *grooves/mm*.　The normal applied voltage of PMT is 800 *KV*.　We used standard fluorescent lamps to calibrate our spectral response of spectrometer and detection system.　The signals of PL spectra are exposed about 0.1*sec* at each step of 0.1nm. The 0.1nm-resolution can be resolved with this monochromator while the entrance and exit slits are both opened about　$50\mu m$.
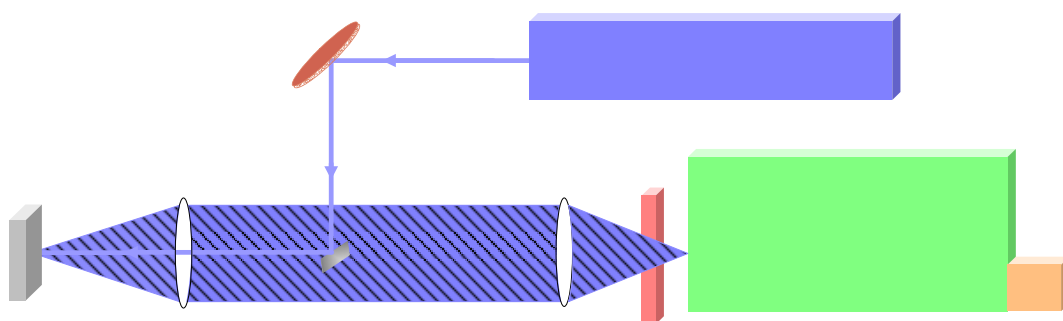

Fig. 3-1 Sketch diagram of photoluminescence spectra

We use the HP-8453 UV-VIS spectrometer for the transmission spectra measurement.　The scan range of the wavelength is from 200nm to 900nm and

increment is 1*nm*. The incident light was perpendicular to the sample and the transmitted light was detected by this transmission spectra.

3-2 Single beam Z-scan apparatus

The apparatus of single beam Z-scan is shown in Fig. 3-2. A tunable Kerr-lens mode-locked Ti:sapphire laser (coherent Mira 900-F) with repetition rate of 76*MHz* was used as the exciting source. The laser has nearly Gaussian spatial mode distribution and the full width at half maximum pulsewidth around 175-*fs*. The incident light is chopped by a chopper with 1.33 *KHz* frequency and divided by a polarization beam splitter into two beams. The reflected beam was detected by the photodiode as the reference light. The transmitted beam, as the exciting light, was focused by a 50*mm* focal-length lens and the beam radius ω_0 of focused is around 17-18 μm at the focus point. Our sample was mounted on a step motor and moved along the z direction with 1.25 μm movement per step. A finite aperture was placed in the far field to control the transmittance of the light in the z-scan measurement. The signal are simultaneously detected by two photodiodes and sent to a lock-in amplifier (Model: SR830) to increase the signal-to-noise ratio. First, the aperture was opened completely to obtain the open aperture z-scan trace (S=1) which implies nonlinear absorption and then aperture was reduce to gain the closed-aperture z-scan trace (S=0.4) which contains nonlinear absorption and refraction. To purely obtain the nonlinear refraction, a simple division of the closed-aperture trace by open-aperture trace will be performed. The divided Z-scan curves exhibit the expected features, namely, a valley-peak (*v-p*) for the positive nonlinearity and a peak-valley (*p-v*) for the negative one. An irradiance-dependent Z-scan study will

be performed to investigate the nonlinear refraction caused by two photon absorption (2PA) generated free carriers, an effective fifth-order nonlinearity, and an wavelength-dependent Z-scan will be presented for the resonance behaviors.

For the measurements of single beam Z-scan with exciting wavelength of near UV light, we use BBO crystal to make frequency doubling and the following procedure is the same with Fig. 3-2.
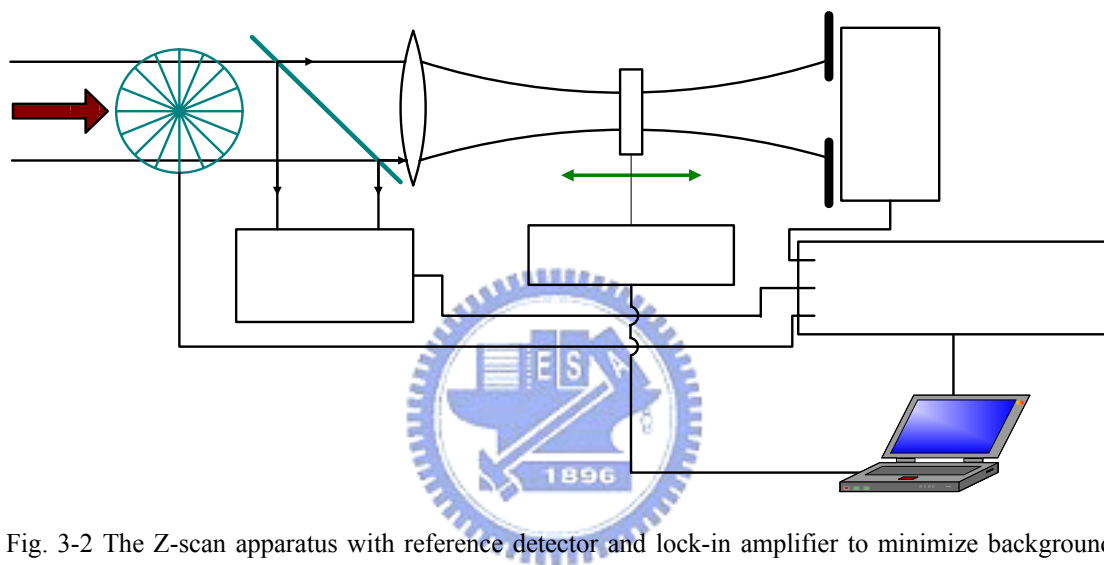

Fig. 3-2 The Z-scan apparatus with reference detector and lock-in amplifier to minimize background and maximize the signal-to-noise ratio respectively.
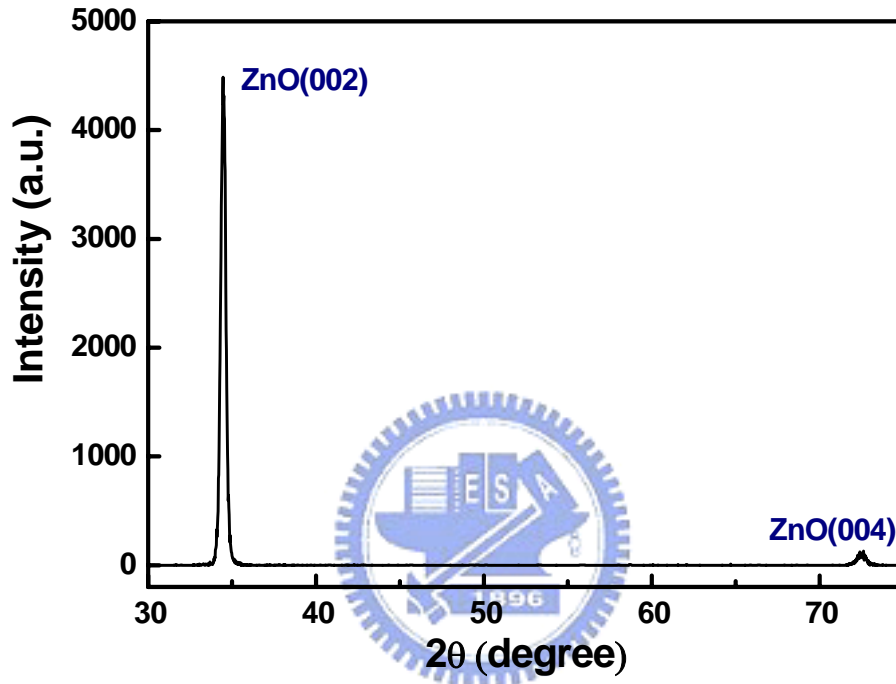
Chapter 4 Results and Discussions

4-1 XRD

Fig. 4-1 Result of X-ray diffraction measurement

The thickness of ZnO thin film was about 1 μm by surface profile measurement offered by Nano Facility Center (NFC) at NCTU. Result of X-ray diffraction measurement is shown in Fig. 4-1 which offered by a JAP MAC Science MXP18 X-ray diffractometer at NTHU. By comparing with JCPDS#36-145 and our diffraction pattern in Fig. 4-1, a strong diffraction line was observed only from the (002) and (004) planes. This result indicates that the ZnO sample is single crystalline thin film with the crystallographic c-axis being parallel to the growth direction (perpendicular the surface of this sample).

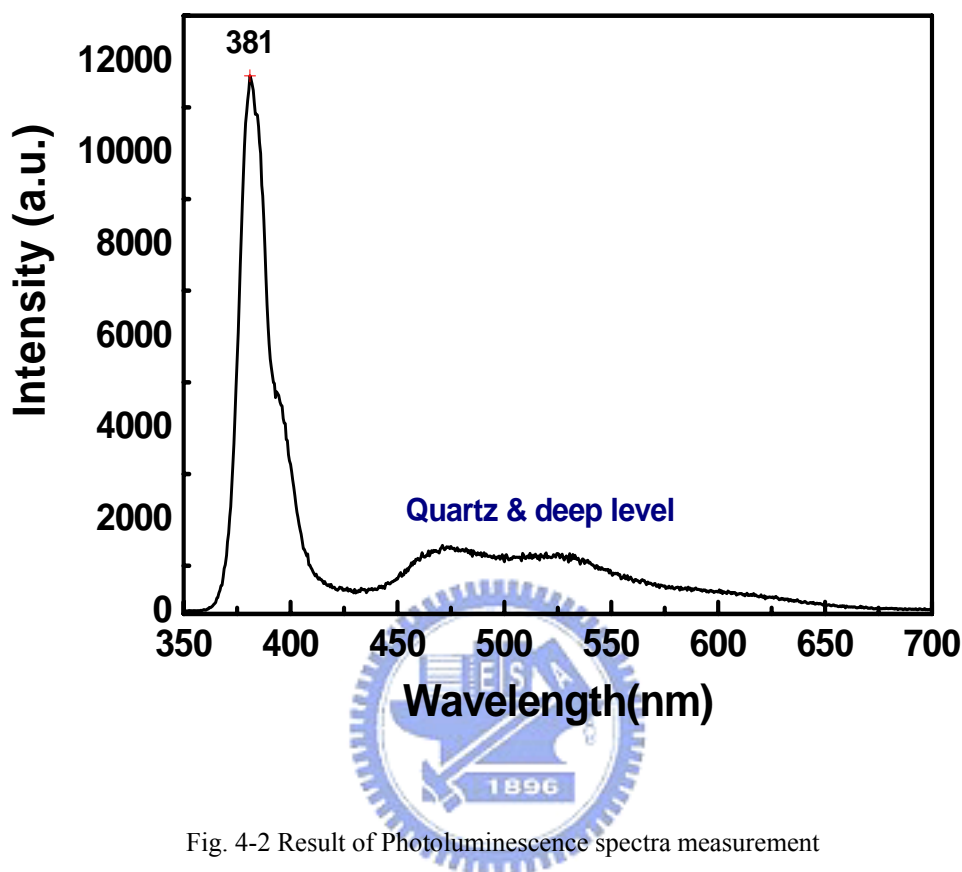## 4-2 Photoluminescence Spectra

Fig. 4-2 Result of Photoluminescence spectra measurement

With using the PL spectra shown in chapter 3-1, the near-band edge emission and deep-level emission of this ZnO thin film can be investigated.   As Fig. 4-2 shows, the near band edge emission of this ZnO thin film is around 381*nm*.   However, the main features of PL spectra at room temperature are similar for most of epitaxial ZnO samples.   The broad band emission of 450*nm*-550*nm* is contributed from the substrate of fused silica and deep level of ZnO.   This is due to lattice mismatch of fused silica and ZnO.   This broad band emission can be reduced by replacing the substrate of fused silica by double-side polished sapphire.   But this kind of sapphire substrate can contribute the nonlinear absorption and refraction when the wavelength of incident pulse is near two-photon resonance of ZnO thin film [26].   It will lead

some errors in calculation of nonlinear absorption and refraction of ZnO thin film. Moreover, this contribution of deep level of ZnO is tenfold smaller than the near-band edge emission; thus it will not induce a large amount of other nonlinearities in Z-scan measurements due to defect level.
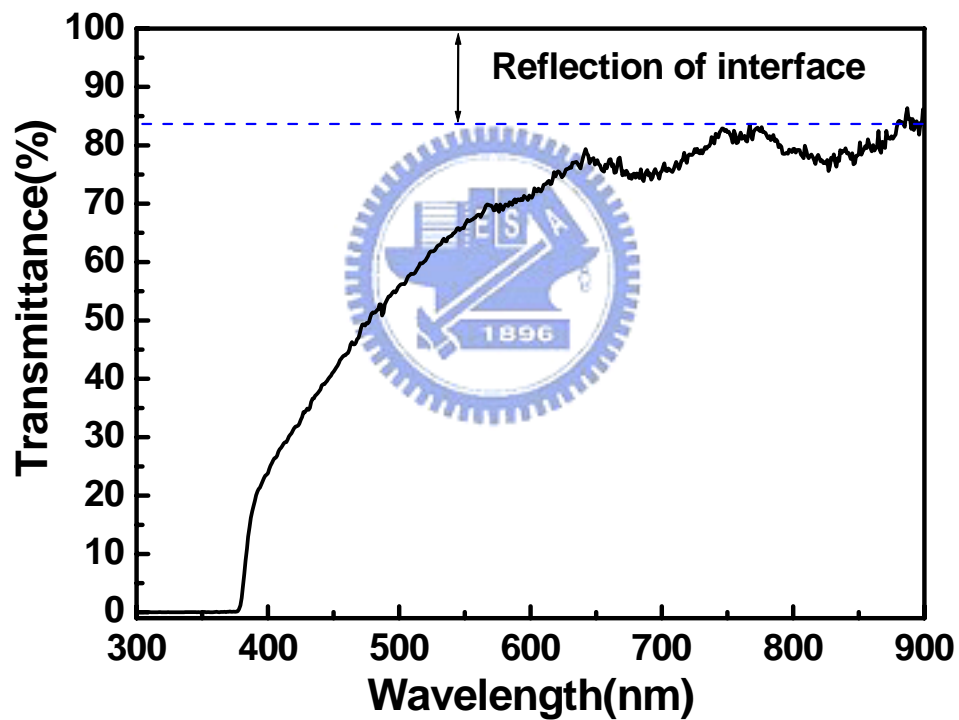
4-3 Transmission Spectra

Fig. 4-3 Result of transmission spectra measurement

High transmittance is necessary for Z-scan measurement. From Fig. 4-3, the transmittance of ZnO thin film is close to 82% between $700nm$ and $900nm$. By taking into account the reflection at air-film, film-substrate and substrate-air interface

of total 16.6%, the absorption and scattering is less the 1.4%. Besides, a simple

formula $d = \dfrac{\lambda_1 \lambda_2}{2(n_2 \lambda_1 - n_1 \lambda_2)}$ can be used for the calculation of sample thickness via

transmission spectra for our measurement where n_1 and n_2 are the refractive indices at

two adjacent maxima (or minima) at λ_1 and λ_2. By applying $\lambda_1 = 642nm$,

$\lambda_2 = 759nm$ and $n_1 = 1.98$, $n_2 = 1.96$, we can evaluate sample thickness d is about

1023nm which is close to the result of surface profile measurement.

4-4 Measurement of Z-scan

4-4-1 Z-scan in the range of near IR

A series of measurement results of Z-scan for a $1\mu m$ high-quality c-axis

oriented ZnO thin film which was grown on a fused silica substrate by laser MBE has

performed. Fig. 4-4 (a) shows the Z-scan measurement with the open aperture (solid

squares), and closed aperture (solid circles) by the excitation of $I_0 = 1.93$ (GW/cm^2)

and $\lambda = 740nm$. In the fully open-aperture Z-scan trace (S=1), the characterization of

two photon absorption is displayed that is having a deep and is symmetric relative to

the focal point ($z=0$). The shape could be a deep or a peak due to the multiphoton

absorption or linear absorption saturation. The two photon absorption coefficient

$\beta = 701.67 \pm 11.05(cm/GW)$ at the 740nm of exciting wavelength can be obtained

from the data of S=1 by fitting curve with equation (14) of chapter 2. The

valley-peak characterization with an enhanced valley resulting from the two photon

absorption is showed in closed-aperture (S=0.4) Z-scan trace which may present a

positive nonlinear refraction. The normalized transmittances are not equal in far away the prefocal and postfocal positions that may come from the vibration of laser power and the photoluminescence of sample (Fig. 4-4 (a), S=0.4). In order to exclude the two photon absorption from the closed-aperture, we can gain a symmetric valley and peak Z-scan trace as shown in Fig. 4-4 (b) by dividing the S=0.4 by the S=1. While we neglected the free carrier nonlinearity, the nonlinear refraction coefficient $\gamma = 2.45 \pm 0.07 \times 10^{-11} (cm^2/W)$ can be obtained by fitting Fig. 4-4 (b) with equation (10) of chapter 2.
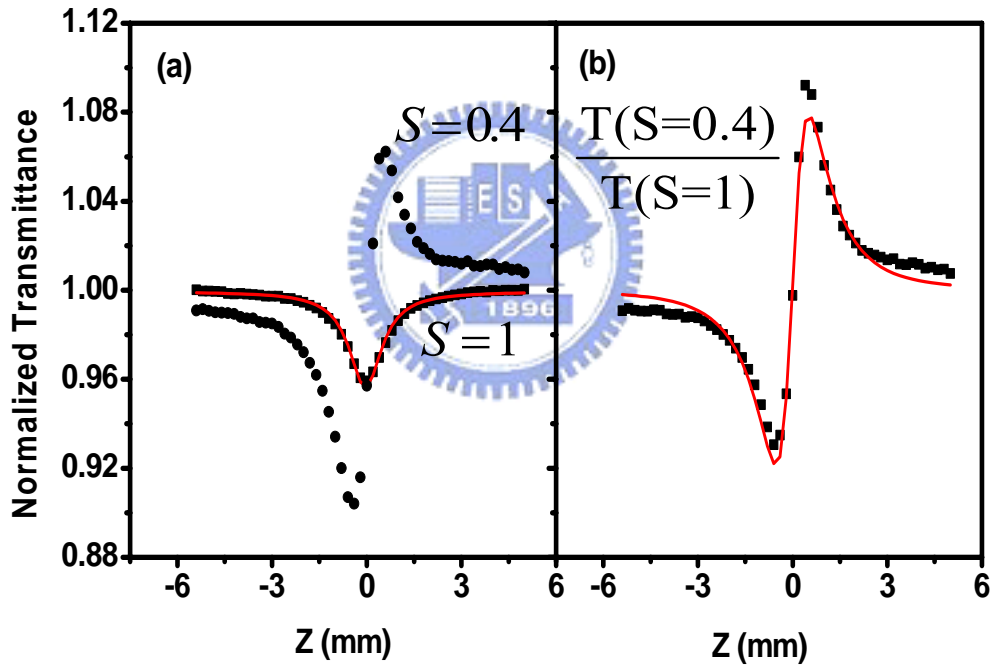

Fig. 4-4 Result of Z-scan with excitation by I_0=1.93 (GW/cm^2) and λ=740nm for ZnO thin film (a) S=1(solid squares) and S=0.4(solid circles) (b) the divided result. The solid line is fitting result by theory.

A series of symmetric normalized Z-scan traces versus the different laser peak irradiance are shown in Fig. 4-5. The normalized transmittance difference between

peak and valley (ΔT_{p-v}) gradually increases as increasing the peak irradiance. In this section, we try to fit the nonlinear phase shift $\Delta\Phi$ by using the equation (10) of chapter 2 and the change of nonlinear refraction Δn can be obtained with the relation of $\Delta\Phi = \dfrac{2\pi}{\lambda}\Delta n \dfrac{1-\exp(-\alpha L)}{\alpha}$. Here, λ is the wavelength of incident laser, α=705.53cm^{-1} is the linear absorption coefficient of ZnO thin film and L=1μm is the thickness of sample. Because of Δn is a polynomial of ascending power, Δn increasing with peak irradiance result in the increase of ΔT_{p-v}. Table III shows the fitting results of Z-scan for λ=740nm.

	$I_0 (GW/cm^2)$	$\Delta\Phi$	Δn	$\Delta n/I_0$
1	0.69	0.127	0.016	0.023
2	0.981	0.188	0.023	0.023
3	1.158	0.215	0.026	0.023
4	1.591	0.357	0.044	0.027
5	1.758	0.333	0.041	0.023
6	1.928	0.387	0.047	0.024
7	2.134	0.395	0.048	0.023

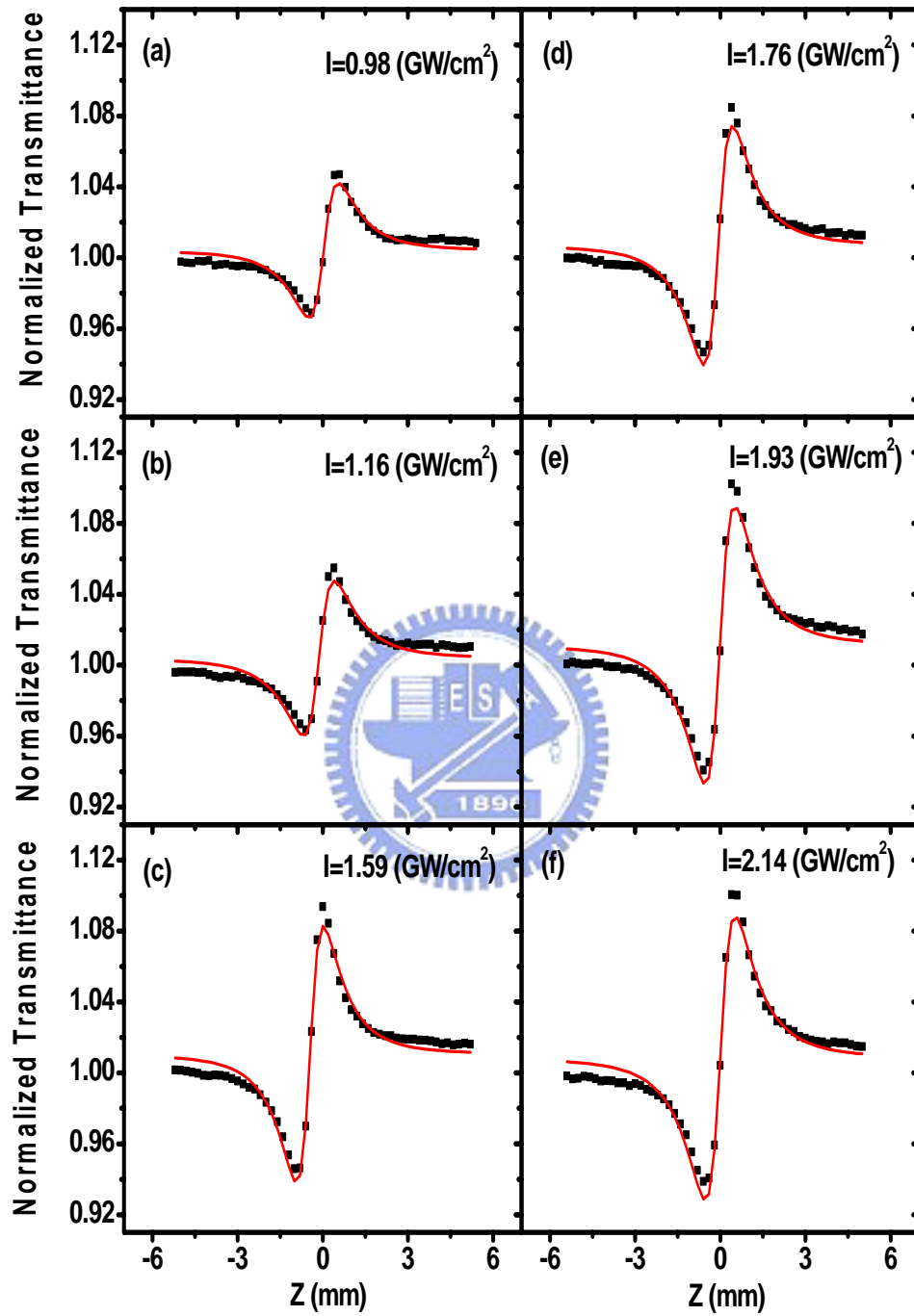Table III   The fitting results of Z-scan for λ=740nm.

Fig. 4-5 The results of closed-aperture divided by the open aperture with different laser peak irradiance and 740*nm* laser excitation.   The solid line is the fitting result by theory.

The irradiance independent two photon absorption coefficients β while the wavelength of excitation laser at 740nm is shown in Fig. 4-6. The distribution of β versus the irradiance appears to be flat with the average value of $732.08 \pm 4.21(cm/GW)$ and an uncertainty of 0.6% arising from the perturbation of laser wavelength. This flat tendency also implied that two-photon absorption process is intrinsic third-order nonlinearity.
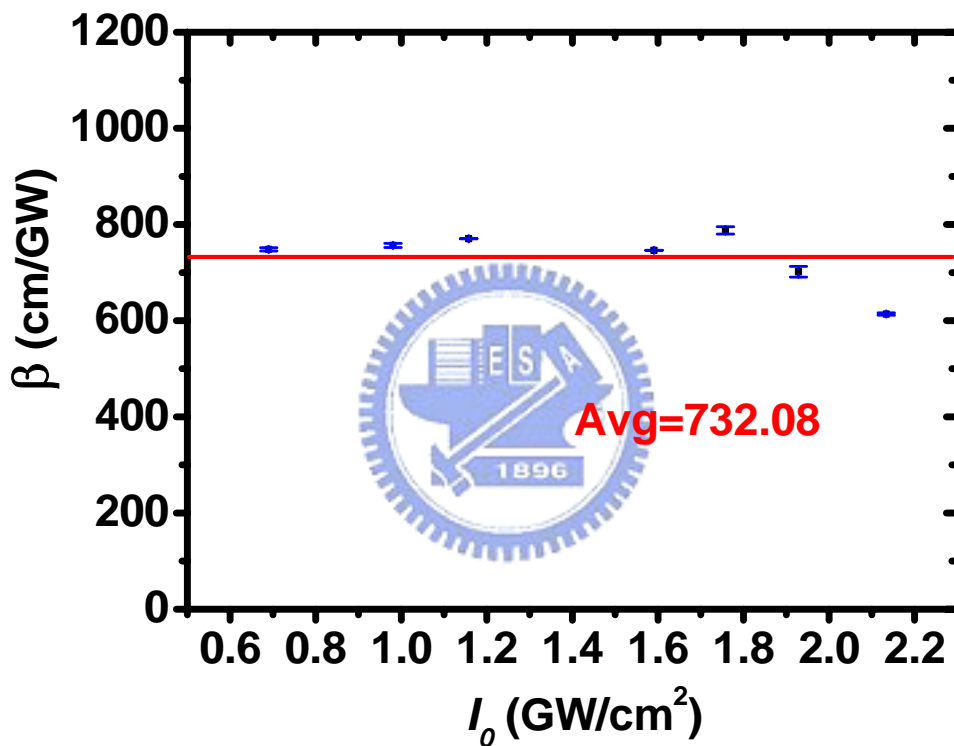

Fig. 4-6 Two photon absorption coefficient with different peak irradiance and 740nm laser excitation. The horizontal solid line is a guide for the eye and yields the average value $\beta = 732.08 \pm 4.21(cm/GW)$.

If the strength of change of nonlinear refraction Δn is due to bound electronic effect and two-photon absorption generated free carrier, the $\Delta n/I_0$ can be written as follows by A. A. Said et al [27]

$$\Delta n / I_0 \simeq \gamma + C\sigma_r I_0 , \tag{32}$$

where C is given by $C \simeq 0.23(\beta t_0 / \hbar \omega)$ for low linear absorption ($\alpha_0 L < 0.2$), γ is the nonlinear refraction index and σ_r is the refractive-index change per carrier-pair density. Therefore, we can obtain the γ and σ_r by plotting the relation of $\Delta n / I_0$ versus I_0 from experimental data and making a curve fitting with equation (32). The free carrier nonlinearity σ_r can be obtained from the slope of fitting straight line by calculating the constant C. The interceptive value of the fitting straight line with y-axise represents bound electronic nonlinear refraction index. Fig. 4-7 shows the experimental measuring result of $\Delta n / I_0$ versus I_0 (solid squares) while the laser excitation is at 745nm. By a curve fitting with equation (32), the parameters $\gamma = 2.27 \pm 0.1 \times 10^{-11}(cm^2/W)$ and $\sigma_r = 9.28 \pm 1.6 \times 10^{-20}(cm^3)$ can be obtained from the intercept and slope of straight line. The average value of $\beta = 297 \pm 1.1(cm/GW)$ is small than the value of the β at 740nm due to the reason that 745nm is near the half bandgap and 740nm is above half bandgap. Both of β at 740nm and 745nm are independent of peak irradiance.

In our measurements, the two photon absorption coefficient, bound electronic and free carrier nonlinearity show strong enhancement than that reported in references [28] [29]. By using the single beam Z-scan technique with the mode-locked (25ps) frequency doubling Nd:YAG laser (532nm) as the pumping source, the nonlinear properties of 1mm ZnO single crystal are measured and the result of $\beta = 4.2cm/GW$, $\sigma_r = -1.1 \times 10^{-21}cm^3$ and $\gamma = -0.9 \times 10^{-14}cm^2/W$, respectively. Furthermore, the third-order optical nonlinearity of ZnO microcrystallite thin films near the excitonic resonance has also been measured at various temperatures using the femtoseocnd degenerate four-wave-mixing technique and revealed an excitonic enhancement of $\chi^{(3)}$ [30]. The values of $\chi^{(3)}$ range from 10^{-6} to 10^{-8} esu at room temperature.
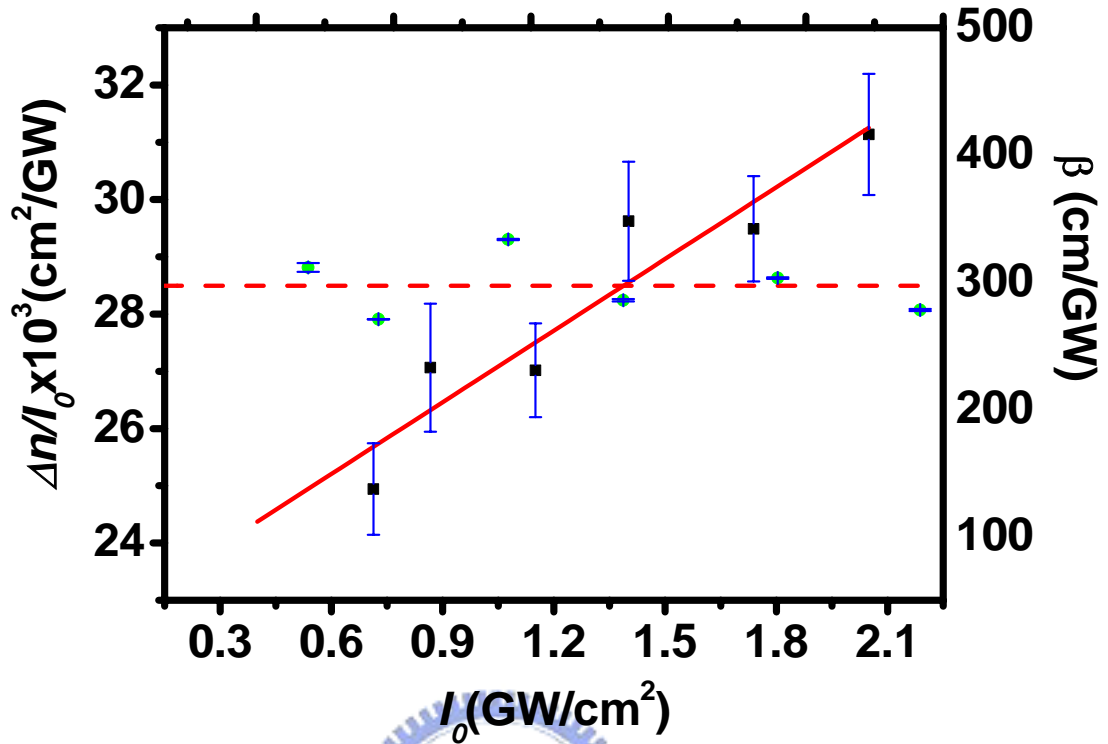
Fig. 4-7 Two photon absorption coefficients (solid circles) versus peak irradiance and $\Delta n / I_0$ (solid squares) plotted as a function of peak irradiance I_0 for ZnO thin film with 745*nm* laser excitation. The horizontal dashed line is a guide for eye and the average value of β is 297±1.1(*cm/GW*). The intercept of fitting straight line gives $\gamma = 2.27 \pm 0.1 \times 10^{-11}(cm^2 / W)$ and the slope yields $\sigma_r = 9.28 \pm 1.6 \times 10^{-20}(cm^3)$.

We believe that the enhancement of the two photon absorption in our experimental results come from the excitonic effect. In order to investigate the behavior of excitonic resonance, a wavelength-dependent β in Z-scan measurement is shown in Fig. 4-8. It is obvious that two enhancements of the β is obviously seen when the exciting wavelength is at 760*nm* and below 745*nm* from Fig. 4-8. In ZnO, the exciting beam of 745*nm* is close to the one-half bandgap energy ($1/2E_g$) and the wavelength of 760*nm* is near the one-half resonance of the excition energy level that equals to half bandgap energy minus half exciton binding energy ($1/2E_g$-$1/2E_b$). It is also confirmed from the PL result of room temperature.
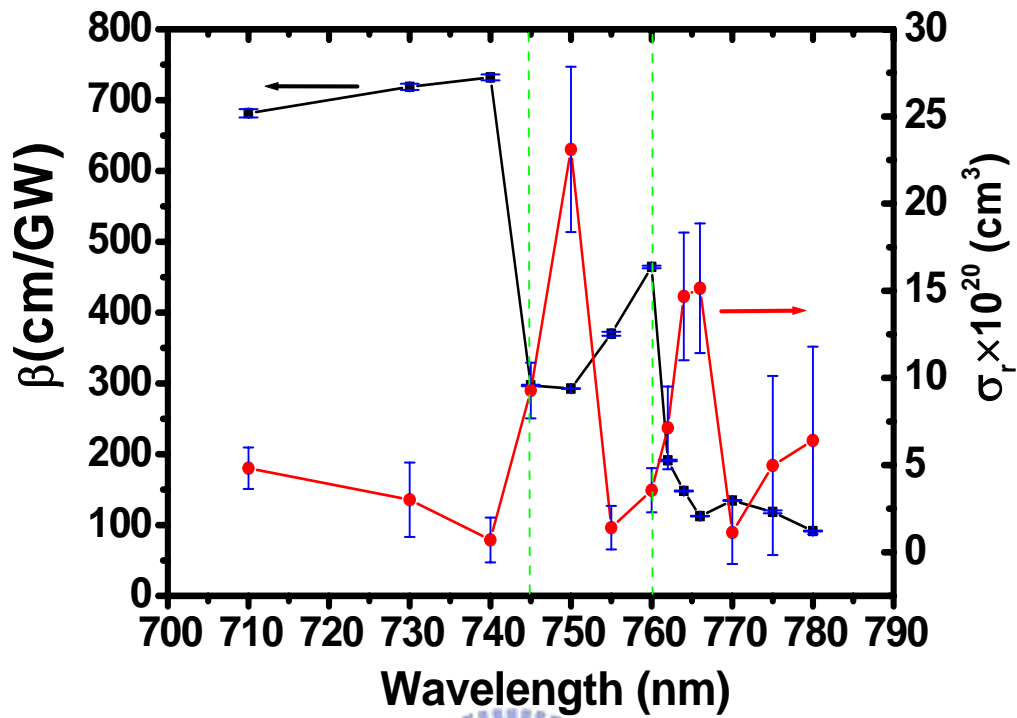
Fig. 4-8 σ_r (solid circles) and β (solid squares) versus wavelength for ZnO thin film.   It reveals a red shift of resonant peaks of σ_r related to β.

Therefore, the β declines apparently while the exciting wavelength is longer than the 740nm and then increases while the wavelengths of incident laser above 750nm. Above the 760nm, the β decreases rapidly and tends to a constant due to off the two-photon resonance.   The excitonic enhancement behavior could also be observed in GaN thin film [18].   In the GaN thin film, the peak value of two photon absorption coefficient is 1500 (cm/GW) which reveals an enhancement factor >100 than the values ~ 15 (cm/GW) [31] below bandgap.   Because of the exciton binding energy in GaN thin film is 27meV but 60meV in ZnO thin film.   In addition, the thermal energy is about 26meV and therefore the excitonic effect still exists in ZnO thin film at room temperature.   Compared our experimental results with ZnO single crystal measured at 532nm [28], there is an enhancement factor >120 of β when the

wavelengths of incident laser are 760*nm* and below 745*nm*.

Fig. 4-8 also shows the relationship between free carrier nonlinearity σ_r and wavelength. It is obvious that two resonant peaks exist when the wavelengths of incident laser are 750*nm* and 766*nm*. These two peaks also result from two photon resonance to the bandgap energy and exciton energy level to create free carriers. On the whole, the two resonant wavelengths of σ_r must be equal to that of β because the maximum free carrier density occurred when the two photon absorption attained maximum. However, the resonant wavelengths of σ_r and β are different in our measurements. A red shift of resonant peaks of σ_r related to β is found. We can calculate the energy difference of the two resonant peaks for σ_r and β individually. According to Fig. 4-8, the energy difference between 745*nm* and 760*nm* for β is 32*meV*. Double of 32*meV* is close to 60*meV* which is the exciton binding energy. Therefore, we can define that 745*nm* is the wavelength of half bandgap energy and 760*nm* is the wavelength of half bandgap energy minus half exciton binding energy. The same calculation for σ_r is performed. Double of the energy difference between 750*nm* and 766*nm* is also about 60*meV* which satisfies the exciton binding energy. For this reason, we explain that the origin of two resonant peaks of σ_r come from two photon absorption of 745*nm* and 760*nm*. As for the red shift, it may be due to two photon absorption induced free carrier saturation which is similar to the GaN result [32]. The saturation behavior is clear when the wavelength is below 745*nm*.

We also performed Z-scan measurement while the exciting wavelength is longer than 810*nm*. When the laser wavelengths are operated between 810*nm* and 840*nm*, a peak feature instead of the deep (solid circles) can be seen in the S=1 Z-scan trace as shown in Fig. 4-9 (a). In S=0.4 Z-scan trace (solid squares), a valley-peak feature with the suppressed valley and enhanced peak than the previous measuring result can

be seen in Fig. 4-9 (a). Therefore, a symmetric Z-scan trace from the divided result

of S=0.4 by S=1 is also displayed in Fig. 4-9 (b). This behavior has been

experimentally reported previously and was explained by the linear absorption

saturation [33, 34]. We attribute the peak of the Z-scan measurement to the linear

absorption saturation of ZnO defect states. Absorption saturation function is an

effective negative two photon absorption coefficient β. Following the same fitting

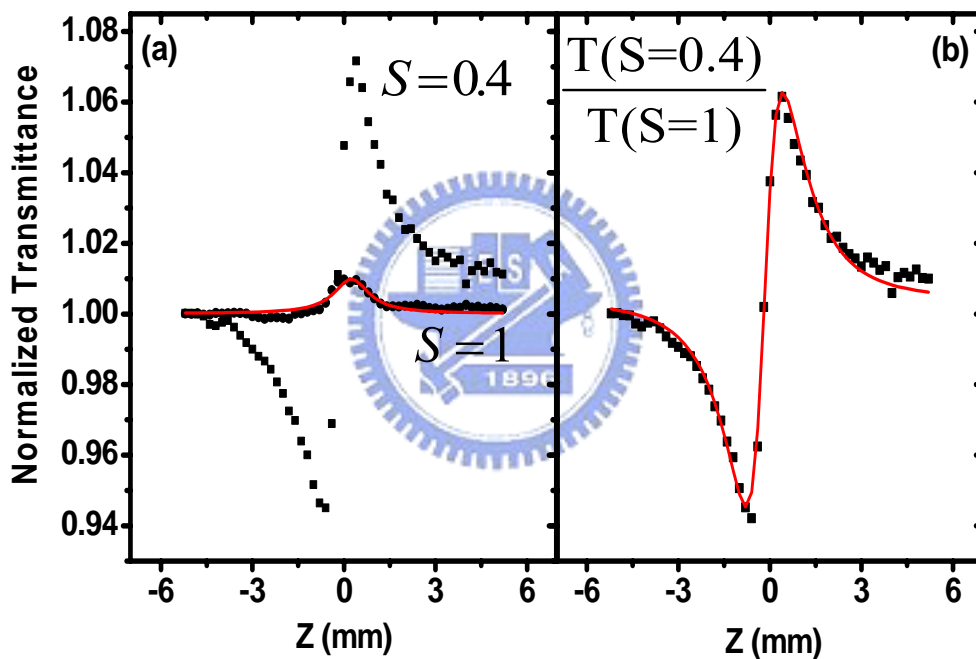procedures, $\beta = -153.13 \pm 9.91 (cm/GW)$ is obtained for λ=830nm.

Fig. 4-9 Result of Z-scan with excitation by I_0=1.855 (GW/cm^2) and λ=830nm (a) S=1(solid circles) and
S=0.4(solid squares) (b) the divided result. The solid line is fitting result by theory.

To experimentally identify the absorption saturation rather than the two photon

excited fluorescence, another experiment similar to the single beam Z-scan

measurement with the optical spectrometer instead of the photodiode is carried out

(Fig. 4-10). The position z dependent transmittance of laser intensity at 810nm from

the spectrometer is recorded by the exciting wavelength of the Ti:sapphire laser at λ=810nm. Similarly to the S=1 Z-scan trace, a peak can be seen when the sample is close to the focus (z=0) as shown in Fig. 4-11 due to the linear absorption saturation of the sample. No fluorescence is found in the experimental setup.
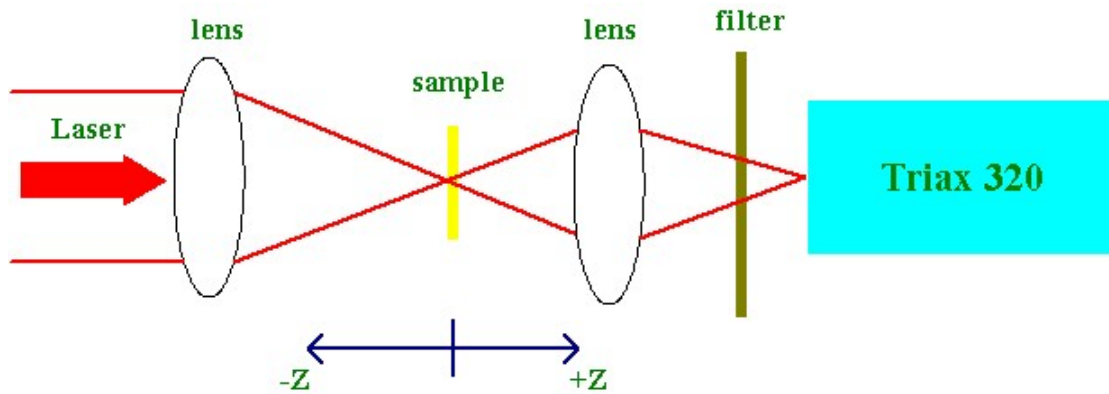

Fig. 4-10 Experimental setup of laser intensity variation dependent on the positions of sample for λ=810nm.
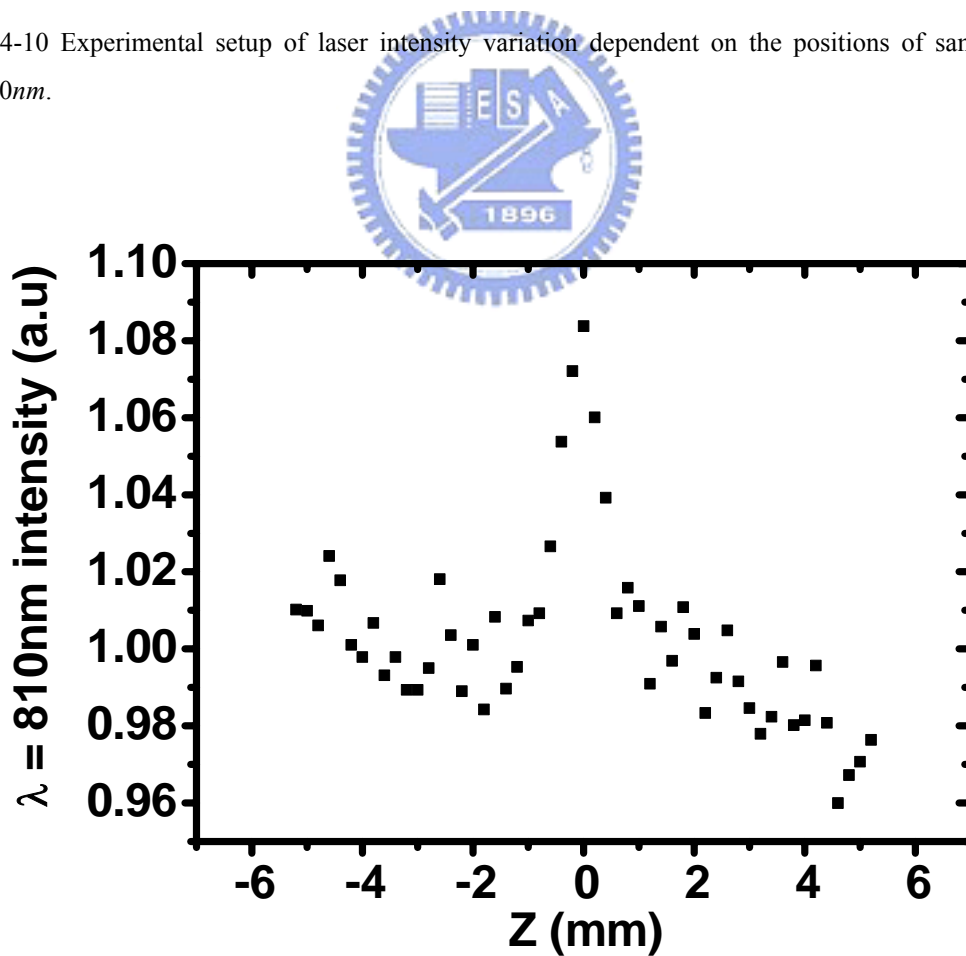

Fig. 4-11 The laser intensity changes with the positions of sample for λ=810nm.
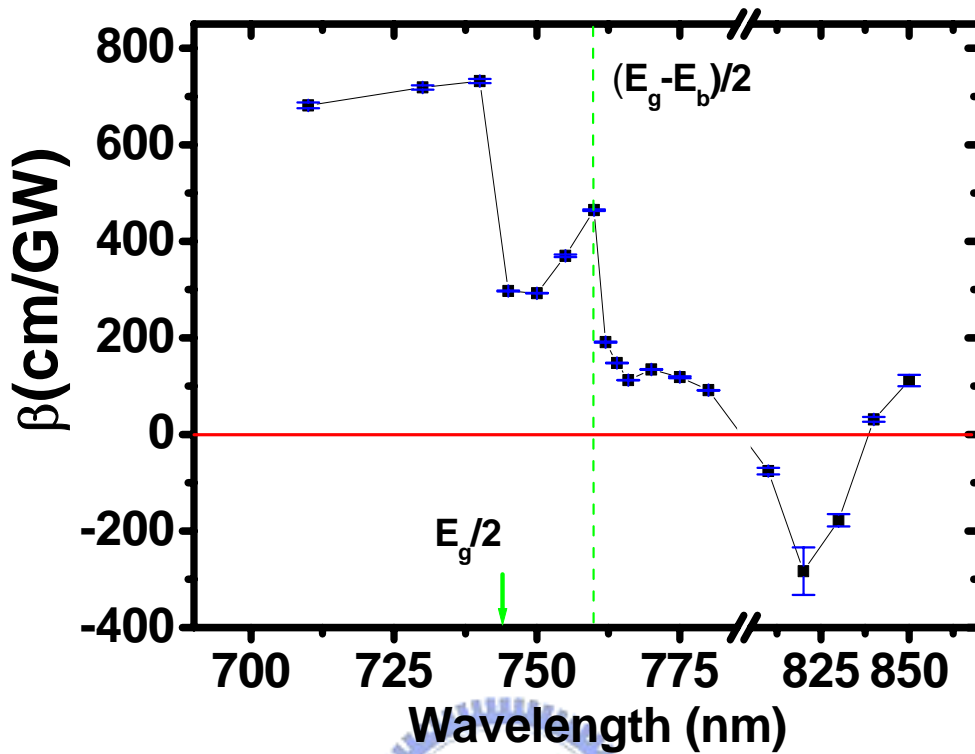
Fig. 4-12 Two photon absorption coefficients versus wavelength for ZnO thin film. It shows the dependence of β and wavelength. Two photon absorption coefficients are enhanced at 760*nm* and below 745*nm* and absorption saturation behavior between 810*nm* and 840*nm* were found.

Fig. 4-12 shows the dependence of β and wavelength. Two photon absorption coefficients are enhanced at 760*nm* and below 745*nm* and absorption saturation behavior were found between 810*nm* and 840*nm*.

The relationship between nonlinear refraction index and wavelength seems irregular as shown in Fig. 4-13. According to the KK relation, the γ will decline following the distribution of the β while the exciting wavelength above 745*nm* but it increases again in the longer exciting wavelength. Besides, the variations of γ are slight in all exciting wavelengths. Because of the high repetition rate of the pulses are used in our measurements, the thermal-optical nonlinearity can not be avoided so that the tendency of γ and β are different. However, the origin of nonlinear

refraction index may mainly result from bound electronic and free carrier effect but the thermal-optical nonlinearity can not be completely neglected. The detail will be further discussed in the next section.
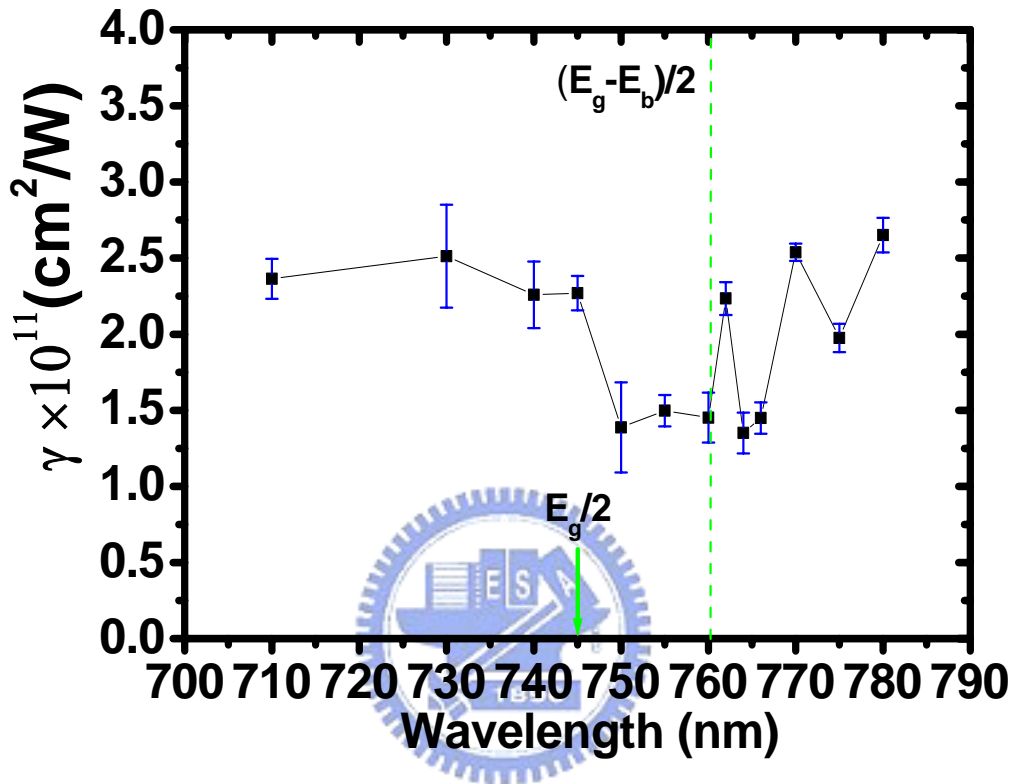
Fig. 4-13 Nonlinear refraction index versus wavelength for ZnO thin film. It seems irregular compared with two photon absorption coefficient.

4-4-2 Z-scan in the range of near UV light

According to the dispersion relation calculated by two-parabolic-band model, the sign of nonlinear refraction index of ZnO thin film will be change from positive to negative when the excitation wavelengths of laser is tuning above $0.7E_g$. The negative Δn has been experimentally demonstrated for ZnO single crystal by the picosecond Q-switching laser with the excitation wavelength at 532*nm* [28]. While

the exciting wavelength below and near E_g of the GaN, the negative Δn of the GaN thin film is also measured by the frequency doubling femtosecond Ti:sapphire pulses [33]. Therefore, we also use UV light as the exciting source by frequency doubling of the Ti:sapphire laser as mentioned in the previous section to perform the Z-scan measurements on the ZnO thin film.

Fig. 4-14 shows the result of Z-scan trace with excitation wavelength of 420nm. The symmetric deep with respect to the focus (z=0) can still exhibit in the open aperture (S=1) Z-scan trace (solid squares) that implies the occurring of the two photon absorption at 420nm. In closed-aperture (S=0.4) Z-scan trace (solid circles), an asymmetric trace relative to the focus with an enhanced deep compared to the open aperture can be seen. As shown in Fig. 4-14 (b), the pure nonlinear refraction index induced Z-scan trace with valley-peak configuration can be obtained from S=0.4 dividing by S=1 that implies Δn is positive. The positive Δn of ZnO thin film under excitation wavelength of 420nm violates the dispersion relation, and therefore we recognize the nonlinearity in this measurement may mainly come from thermal-optical effect due to the high repetition rate of the pulses.

In our measurements, we use a commercial Ti:sapphire laser (Coherent Mira 900-F) as the light source to generate pulses with 76MHz repetition rate and 175fs pulse duration. From the Reference [35], thermal-optical effect occurs if the thermal characteristic time $t_c = \omega_0^2 \rho c_p / 4\kappa$ is longer than the spacing of laser pulses. Here ω_0 is the laser beam radius at the sample, $\rho = 5.67\ g\ cm^{-3}$ is the ZnO density, $c_p = 9.6\ cal\ mol^{-1}\ K^{-1}$ is specific heat, and $\kappa = 0.54\ W\ cm^{-1}\ K^{-1}$ its thermal conductivity [36]. From the parameters above, we estimated that t_c is about $1.3\mu s$ for our measuring of the ZnO thin film which is much longer the spacing of laser pulses ~ $0.013\mu s$. Therefore, thermal-optical effect may not be eliminated in our
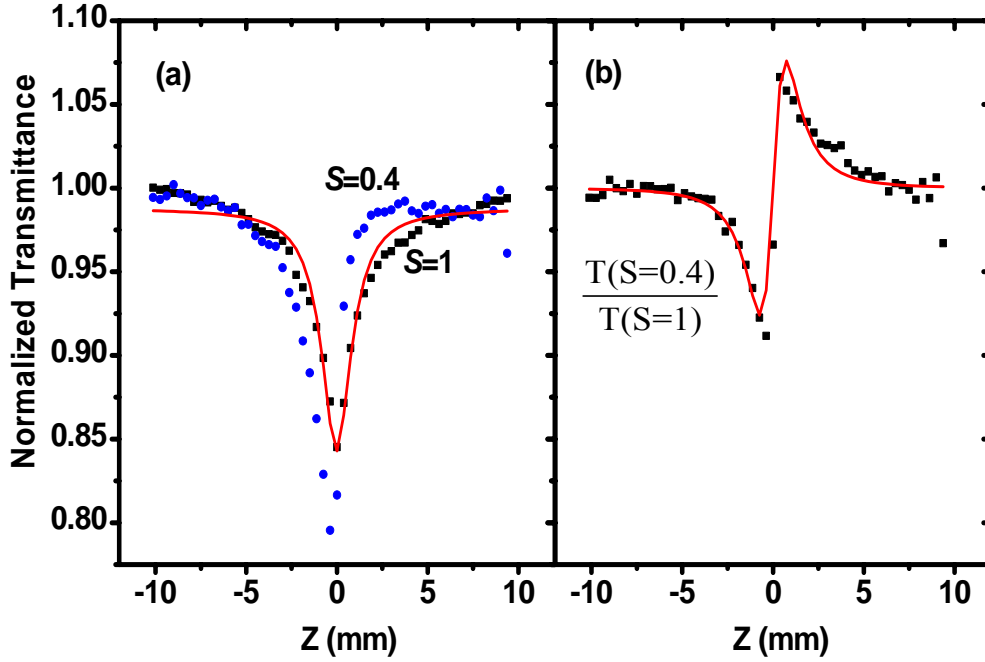
Fig. 4-14 Result of Z-scan with excitation by $\lambda=420nm$ for ZnO thin film (a) S=1(filled squares) and S=0.4(filled circles) (b) the divided result. The solid line is the best fitting and the nonlinear refraction index reveals a positive sign.

closed-aperture Z-scan measurement by the high repetition rate of the pulses. In order to analyze the thermal-optical effect, we use equation (25) of chapter 2 as the fitting formula to obtain the parameter of q and nonlinear absorption coefficient β. By the fitting result shown in Fig. 4-14 (b), we can get $q = 2.07 \pm 0.08$ that is excellent consist with the hypothesis of two photon absorption and implies the origin of thermal-optical effect. The other parameter $\vartheta(q) = 0.51 \pm 0.05$ can also be obtained by the curve fitting that can be used to obtain the two photon absorption coefficient (β_{cal}) by the relation $\beta_{cal} = 2N\sigma(2)/h\upsilon$. If the valley-peak configuration in Fig. 4-14 (b) is induced by heat due to the positive sign of thermal-optical coefficient $dn/dT(K^{-1}) = 0.7\times10^{-4}(K^{-1})$ in ZnO [37], the $\beta_{cal} = 2.2 \pm 0.2\times10^{5}(cm/GW)$ is estimated. Similarly, we also obtained

$\beta_{fit} = 4.79 \pm 0.17 \times 10^4 (cm/GW)$ from S=1 in Fig. 4-14 (a) by the curve fitting with

equation (14) of chapter 2 and linear absorption coefficient $\alpha = 31000 cm^{-1}$.

Although β_{cal} is about five times larger than β_{fit}, we recognize the two values are

similar and the difference may come from curve fitting and the inaccuracy of the

calculated parameters. Noted that the measured values of β_{cal} and β_{fit} in the UV

range are much larger than the value measuring near IR due to the near one photon

resonance. The values of β_{fit} are $5.09 \pm 0.09 \times 10^4 (cm/GW)$ and

$5.87 \pm 0.22 \times 10^4 (cm/GW)$ at the exciting wavelength of 400nm and 390nm,

respectively. Apparently, the value of β_{fit} increases gradually while the excitation

wavelengths are operated close to the band-edge of ZnO thin film.

The fitting formula due to the thermal-optical effect is also applied to the S=0.4

Z-scan data in the near IR range that are listed in Table IV. The wavelength

dependent parameter *q* (number of photon absorption) is plotted in the Fig. 4-15.

The two-photon absorption are indirect verified for the fitting values of *q* greater than

two while the exciting wavelengths near the IR (710nm~780nm). While the exciting

wavelengths are longer than 810nm, the values of the *q* smaller than 2 consist with the

previous measuring result of the absorption saturation that is due to the linear

absorption of ZnO defect states.

The ratios of the β_{cal}/β_{fit} in the different exciting wavelengths are also listed in

the Table IV and plotted in the Fig. 4-15. Note that value of β_{cal} close to β_{fit} (the

ratio is around 5) only occurs while the exciting wavelength at the 420nm and 820nm

and it implies that the nonlinearity induced by nonlinear refraction index is dominated

by thermal-optical effect. In addition, the value of β_{cal} = 220000 (*cm/GW*) at the

420nm is about 175 times larger than the β_{cal} = 1261 (*cm/GW*) at the 820nm due to

near one photon resonance. While the exciting wavelength is operated at the 820nm, the thermal-optical nonlinearity increases due to the linear absorption saturation by the ZnO defect states. The ratio of β is between 10 and 200 from $\lambda=710nm$ to780nm so that we believe the nonlinearity is mainly dominated by bound electronic and free carrier effect. Although the nonlinearity is mainly induced by bound electronic and free carrier effect in near IR range, the thermal-optical effect may have great perturbation. Therefore, the tendency of the γ does not follow the β as shown in the Fig. 4-13 in the previous section. Similar, β_{cal} is more closed to β_{fit} while the excitation wavelengths are near the two photon band-edge and the exciton resonance. Therefore, two deep can be seen as shown in Fig. 4-15.
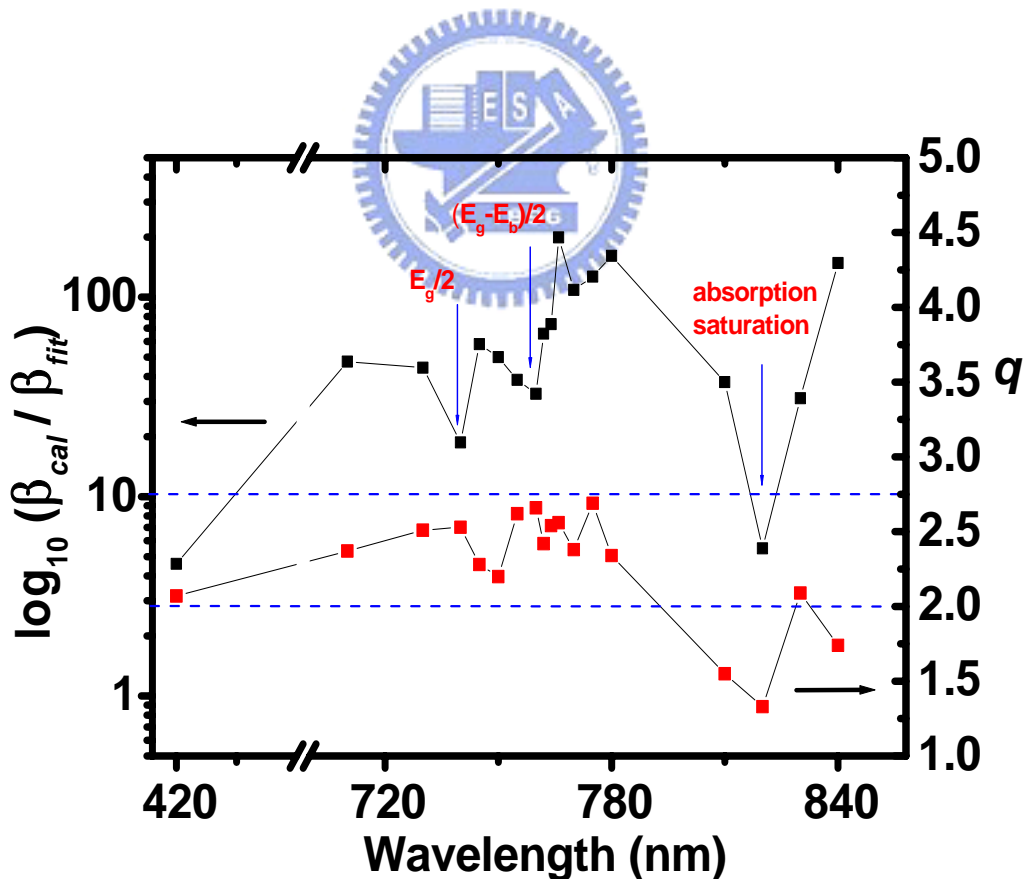

Fig. 4-15 Log$_{10}$(β_{cal}/β_{fit}) and q versus wavelength.

λ (nm)	I_0 (GW/cm^2)	q	$\vartheta(q)$	β_{cal} (cm/GW)	β_{fit} (cm/GW)	β_{cal}/β_{fit}
420	0.35	2.07	0.51	220000	47900	4.6
710	1.325	2.37	0.52	33016	694	47.5
730	1.049	2.51	0.42	30701	693	44.3
740	1.757	2.53	0.61	14741	788	18.7
745	1.401	2.28	0.50	16627	286	58.1
750	1.489	2.20	0.55	12408	248	50
755	1.586	2.62	0.39	13102	340	38.5
760	1.937	2.66	0.60	14934	455	32.8
762	1.435	2.42	0.51	17263	263	65.6
764	2.289	2.54	0.69	10455	143	73.1
766	1.5	2.56	0.43	14752	74	199.3
770	1.667	2.38	0.55	14044	129	108.8
775	2.106	2.69	0.76	14833	117	126.7
780	1.581	2.34	0.56	14357	89	161.3
810	0.793	1.55	0.13	3453	-92	37.5
820	0.861	1.33	0.08	1261	-230	5.5
830	1.598	2.09	0.35	5737	-184	31.1
840	1.053	1.74	0.22	4753	32	148.5

Table IV The fitting results of visible wavelengths by thermal-optical effect.

Chapter 5   Conclusions and Perspectives

5-1 Conclusions

Optical nonlinearities of ZnO thin film made by the laser MBE have been investigated by Z-scan method with the high repetition rate Femtosecond Ti:sapphire laser.   To our knowledge, this is the first time Z-scan measurement of ZnO thin film near one-half bandgap by the exciting wavelength near IR.   Our ZnO thin film is c-axis orientation and well-crystalline with a strong free-exciton luminescence at 380nm that is demonstrated by the XRD and room temperature PL, respectively.   In our Z-scan measurement, the γ and β shows a three-order and two-order enhancement than that in the ZnO bulk measured at 532nm with 25ps pulse duration.   Due to the two-photon resonance at the bandedge and exciton, the β shows an enhancement below 745nm and at 760nm.   Besides, the free carrier induced nonlinearities also shows the similar resonant behavior as the β but a red shift relative to β that might be due to the free carrier saturation.   In addition, an effective negative two-photon absorption coefficient due to an absorption saturation of ZnO defect states is observed while the excitation wavelength above 810nm.   The apparent tendency of wavelength dependent nonlinear refraction can not be seen in our near IR measurements due to the large perturbation from the thermal.

In addition, the positive γ measured at the λ=420nm violates the negative prediction from the two-parabolic-band (TPB) model based on the Kramers–Krönig (KK) relation while the exciting energy above 0.7E_g.   By applying the fitting formula from the thermal optical nonlinearity to the S=0.4 Z-scan data, the parameter of q (number of photon absorption) and β_{cal} (two photon absorption

coefficient) can be gained.   The close values and great increasing of the β_{cal} and β_{fit} than that measured values near IR show that the nonlinear refraction is mainly dominated by the thermal nonlinearity at 420nm.   Furthermore, the large value of the ratio of β_{cal} and β_{fit} in the near IR suggest that bound electronic and free carrier effect is mainly source of the nonlinear refraction index even though the thermal-optical effect can not be neglected.

5-2 Perspectives

Optical nonlinearities enhanced by exciton effect have been performed in ZnO thin film.   The binding energy of free-exciton of ZnO thin film is about 60meV and thermal energy is about 26meV at room temperature.   At higher temperature, the exciton binding energy will be destroyed by thermal energy and the enhanced nonlinearities at low temperature may decrease.   Therefore, a series of temperature dependent Z-scan is necessary in order to further investigate the exciton effect. According to dispersion relation based on the two-parabolic-band (TPB) model, the nonlinear refraction index of ZnO thin film must be the negative value by exciting with the UV light.   Nevertheless, the nonlinearity measured by us is positive by the thermal-optical effect.   For this reason, it is important to reduce thermal influence by lower the repetition rate of exciting laser.   Finally, carrier dynamics is significant for high speed optical devices and therefore a time-resolved Z-scan is required to find the dephaing and cooling time of exciton.

Reference

[1] T. Aoki, Y. Hatanaka, D. C. Look, *Appl. Phys. Lett.* **76**, 3257 (2000)

[2] D. M. Bagnal, Y. F. Chen, Z. Zhu, S. Koyama, M. Y. Shen, T. Goto, *Appl. Phys. Lett.* **70**, 2230 (1997)

[3] H. Cao, Y. G. Zhao, S. T. Ho, E. W. Seelig, Q. H. Wang, R. P. H. Chang, *Phys. Rev. Lett.* **82**, 2278 (1999)

[4] Pertsch T, Peschel U, Lederer F, *Opt. Lett.* **28**, 102 (2003)

[5] Mizrahi, V., Delong, K. W., Stegeman, G. I., Saifi, M. A., and Andrejeco, M. J., *Opt. Lett.* **14**, 1140 (1989)

[6] Fryad Z, Henari, Kai Morgenstern, and Werner J. Blau, *Appl. Phys. Lett.* **67**,323 (1995)

[7] Robert W. Boyd, *Nonlinear Optics*, (1992)

[8] Sheik-Bahae, M. Said, A. A., and Van Stryland, E. W., *Opt. Lett.* **14**, 955 (1989)

[9] Wang, J., Sheik-Bahae, M., Said, A. A., Hagan, D. J., and Van Stryland, E. W., *J. Opt. Soc. Am. B.* **11**, 1009 (1994)

[10] K.Y. Teseng, K. S. Wong, and G. K. L. Wong, *Opt. Lett.* **21**, 180 (1996)

[11] Inuk Kang, Todd Krauss, and Frank Wise, *Opt. Lett.* **22**, 1077 (1997)

[12] Gregory J. Exarhos, Shiv K. Sharma, *Thin Solis Film* **270**, 27 (1995)

[13] Nomura K, Ohta H, Ueda K, Kamiya T, Hirano M, Hosono H, *SCIENCE* **300**,1269 (2003)

[14] Gang Wang, G. T. Kiehne, G. K. L. Wong, and J. B. Ketterson, *Appl. Phys. Lett.* **80**,401 (2002)

[15] H. Cao, J. Y. Wu, H. C. Ong, J. Y. Dai, and R. P. H. Chang, *Appl. Phys. Lett.* **73**,572 (1998)

[16] G. I. Petrov, V. Shcheslavskiy, and V. V. Yakovlev, *Appl. Phys. Lett.* **83**, 3993 (2003)

[17] J.Castillo, V. P. Kozich, and A. Marcano O, *Opt. Lett.* **19**, 171 (1994)

[18] K. H. Lin, G. W. Chern, Y. C Huang, C. K. Sun, *Appl. Phys. Lett.* **83**, 3087 (2003)

[19] M. Falconieri, G. Salvetti, *Appl. Phys. B.* **69**, 133 (1999)

[20] Mauro Falconieri, *J. Opt. A: Pure Appl. Opt.* **1,** 662 (1999)

[21] Gradshteyn I S and Ryzhik I M, *Table of Integrals, Series andProducts 5th edn (New York: Academic)* p933

[22] Sheldon S J, Knight L V and Thorne J M, *Appl. Opt.* **21,** 1663 (1982)

[23] Sheik-Bahae M., D.J. Hagan and E. W. Van Stryland, *Phys. Rev. Lett.* **65**, 96 (1990)

[24] Sheik-Bahae M., Hutchings, D. C., Hagan, D. J., and Van Stryland, E. W., *IEEE J. Quantum Electron.* **27**, 1296 (1991)

[25] T. Y. Wu and T. Ohmura, *Quantum Theory of Scattering.* Englewood Cliffs, NJ: Prentice-Hall (1962)

[26] A. Major, F. Yoshino, I. Nikolakakos, J. S. Aitchison, and P. W. E. Smith, *Opt. Lett.* **29**, 602 (2004)

[27] A. A. Said, M. Sheik-Bahae, D. J. Hagan, T. H. Wei, J. Young, and E. W. Van Stryland, *J. Opt. Soc.*

Am. B. **9**, 405 (1992)

[28] X. J. Zhang, W. Ji, and S. H. Tang, *J. Opt. Soc. Am. B.* **14**, 1951 (1997)

[29] X. J. Zhang, H. Fang, S.Tang, W. Ji, *Appl. Phys. B.* **65**, 549 (1997)

[30] W. Zhang, H. Wang, K. S. Wong, Z. K. Tang, G. K. L. Wong, *Appl. Phys. Lett.* **75**, 3321 (1999)

[31] C. K. Sun, J. C. Liang, J. C. Wang, F. J. Kao, *Appl. Phys. Lett.* **76**, 439 (2000)

[32] Y. C Huang, G. W. Chern, K. H. Lin, J. C. Liang, C. K. Sun, C. C. Hsu, *Appl. Phys. Lett.* **81**, 85 (2002)

[33] Y. L Huang, C. K. Sun, J. C. Liang, *Appl. Phys. Lett.* **75**, 3524 (1999)

[34] R. Rangel-Rojo, S. Yamada, and H. Matsuda, D. Yankelevich, *Appl. Phys. Lett.* **72**, 1021 (1998)

[35] J. P. Gordon, R. C. C. Leite, R. S. Moore, S. P. S. Porto, J. R. Whinnery, *J. Appl. Phys.* **36**, 3 (1965)

[36] Edited by Raneshwar Bhargava, *Properties of Wide Bandgap $II-VI$ Semiconductors*, (1997)

[37] N. Ashkenov, M. Schubert, W. Czakai, G. Benndorf, H. Hochmuth, M. Lorenz, M. Grundmann, Manuscript for possible publication in Phys. Rev. B (Dated: October 25, 2003)